Simulating low-carbon electricity supply for Australia

Manfred Lenzen, ISA, School of Physics A28, The University of Sydney NSW 2006, Australia, m.lenzen@physics.usyd.edu.au
Bonnie McBain, School of Environment & Life Sciences, University of Newcastle, Callaghan NSW 2308, Australia, Bonnie.Mcbain@newcastle.edu.au
Ted Trainer, School of Social Work, University of New South Wales, Kensington NSW 2052, Australia, tedtrainertsw@gmail.com
Silke Jütte, Wirtschafts- und Sozialwissenschaftliche Fakultät, Seminar für Supply Chain Management & Management Science, Albertus-Magnus-Platz, D-50923 Köln, Germany, silke.juette@uni-koeln.de
Olivier Rey-Lescure, School of Environment & Life Sciences, University of Newcastle, Callaghan NSW 2308, Australia, olivier.rey-lescure@newcastle.edu.au
Jing Huang, CSIRO Oceans and Atmosphere Flagship, Yarralumla ACT 2601, Australia, jing.duke@gmail.com

Table of contents

Appendices

A.1 Methods and data

In the following mathematical exposure we let indices e denote energy carrier types, g, d and l geographical grid coordinates of generators, demand points and transmission line segments, and t time. Note also that because electrical energy flows are assessed over a time interval of Δt = 1h, quantities of energy measured in units of MWh are nominally the same as quantities of power measured in units of MW. Our simulations were undertaken in Matlab on a box grid representation of Australia represented by GIS data at a spatial resolution of 0.09 degrees (nearly 9×9 square kilometres). We used a Xeon-processor-based high-performance server configured for large-memory applications running 48 parallel processing cores at speeds of ≥3 GHz using 2 Terabytes of shared system memory. A sparse tensor toolbox (Bader and Kolda 2007) was used to reduce RAM requirements for the largest simulation arrays.

We use gridded data on half-hourly wind speed, air-mass-adjusted solar irradiance (global, direct beam and diffuse) and the beam irradiance fraction were supplied by Huang 2014. These data were produced by dynamically downscaling an ERA-Interim global re-analysis of the European Centre for Medium-Range Weather Forecasts (ECMWF), using CSIRO's Conformal Cubic Atmospheric Model (CCAM). CCAM is a global forecasting model supporting a variable-resolution global grid through the use of Schmidt transformation (see McGregor 2005, and McGregor and Dix 2008). Therefore, it is able to focus on a target area with a fine grid spacing while avoiding the need for any special treatment of simulation boundaries. This dataset has been validated by observation time series from various stations across Australia (Huang 2014). Huang (2014) also demonstrated that its accuracy is comparable to satellite-derived irradiance data on daily global irradiance while it is available for a longer time period, making it ideal for the study of wind and solar resource assessment.

The quality of our irradiance data should be comparable to the 10-km and 1-hour scale satellite-derived BoM data used in the work by Elliston *et al.* 2012. The differences between the two data sources are confined to short-term ramp rates (variability) for single sites. These differences should not have a major influence on simulation results, given that the extent of variability quickly decreases with spatial coverage. Elliston *et al.* 2012 use AEMO wind speed data from selected wind farms, whilst we use results from continental weather simulations. On one hand, real wind farm data are realistic, however they are valid only for the particular data recording sites. We believe that a simple scale-up of a small number of sites is quite problematic in representing national wind power potential, which in turn is better assessed using wind speed data covering the whole of Australia. More importantly, continental data are indispensable for simulations where sites and capacity of wind generators are determined endogenously.

A.1.1 Optimisation

Minimising overall system cost subject to meeting demand can be written (ignoring any indices) as

$$\begin{aligned} &\min z = z_C + z_F + z_V + z_L + z_T \\ &\text{subject to } PT(t) \geq OU(t) \geq DM(t)\frac{(1-LOLP_{\max})}{(1-TL)}, \end{aligned} \quad \text{(A1.1)}$$

where z are overall system cost over an entire modelling period, z_C are capital cost, z_F and z_V are fixed and variable operating and maintenance cost, z_L are fuel cost, and z_T transmission cost. The constraint means that, at every hour, generated output OU must be smaller than the resource potential PT, but at least as large as demand DM minus the maximum loss-of-load (occurring at probability $LOLP_{\max}$) plus transmission losses TL. More specifically (compare with Section 7 in Short *et al.* 2011), for a modeling period of T hours,

$$z_C = \sum_{eg} CC_g^e \; CP_g^e \frac{(1+\delta\iota)T}{LT^e}, \quad \text{(A1.2)}$$

where CC_g^e are the specific capital cost for a capacity unit of plant using energy carrier e (Tab. 1), CP_g^e is the capacity of energy carrier e deployed at location g, LT^e holds plant lifetimes in hours (Tab. 1), ι and δ are the assumed interest rate and debt fraction (Short *et al.* 2011, Tab. 9). Similarly, fixed operation and maintenance cost are

$$z_F = \sum_{eg} CF_g^e \; CP_g^e \; (1+\delta\iota)T, \quad \text{(A1.3)}$$

where CF_g^e are annual fixed operation and maintenance cost, converted into hourly values (Tab. 1). Variable and fuel cost accumulated over the modelling period T can be written as

$$z_V + z_L = \sum_{egt} \left(CV_g^e + CL_g^e\right) OU_g^{et}, \quad \text{(A1.4)}$$

with CV_g^e and CL_g^e expressed per unit of generated output (Tab. 1). Costs for additional transmission capacity are

$$z_T = \sum_l \pi_k(k_l)\sqrt{\Delta a}, \quad \text{(A1.5)}$$

where $\pi_k(k_l)$ the specific cost of a unit length of transmission line required in grid box l at a rated capacity k_l, and $\sqrt{\Delta a}$ = 38.6 km is the linear size of a grid box.

Many of the quantities in Eqs. A1.1-A1.4 are decision variables. Assessed on a 100×100-box grid, for 12 months or 8760 hours, and for 12 energy carriers, generated output OU_g^{et} alone would comprise more than 1 billion elements. Optimising the transmission network is an even more difficult nonlinear combinatorial problem involving the risk of explosion of the number of alternatives in the search space (Romero *et al.* 2002). Since such problems are clearly of prohibitive size for available solvers, researchers make certain

simplifications and reduce the problem so it becomes solvable. Short *et al.* 2011 simplify the year-long modelling period to 17 time slices, characterising each slice by typical resource potentials and probabilities describing resource variability. Similarly, Huva *et al.* 2012 explain how large weather data and RAM requirements of their downward-gradient optimisation technique prevented both an hourly run over a whole year, as well as the utilisation of every geographical grid point available. They create a pseudo-year by splicing together seasonal snapshots in order to reduce runtime, and apply site pre-selection methods. Jägemann *et al.* 2012 account for different demand structures by selecting three days for each of the four seasons, as well as 130 regions in their simulation of decarbonisation pathways for Europe. Elliston *et al.* 2012 model hourly, but restrict their modelling runs by pre-specifying generator sites and capacity. Mason *et al.* 2010 also model hourly, but treat New Zealand as one demand location and thus do not attempt spatial resolution. The AEMO 2013 report describes hourly modelling, but a reduction of spatial resolution to 43 locational polygons in order to deal with the complexity. There is hence limited spatial optimisation present in the latter studies.

The philosophy pursued in this work is for as many parameters as possible to remain variable. We allow full generator site and energy carrier choice for the optimisation problem, and we do not prescribe any merit order. We implement a multi-step hourly selection process narrowing down the generator location search space, by emulating an hourly competitive bidding process with bids set to equal variable plus fixed cost for a unit MWh of output plus transmission losses. The successful generator is therefore not necessarily one with the lowest operating cost, but also determined by the proximity to the demand point. In a first step, supply is matched optimally (ie lowest cost) to demand, iteratively for each single hour of the simulation period. For 12 energy carriers on a 90×110-box grid, the hourly decision variable OU_g^{et} counts about 120,000 elements, which is well manageable on current HPCs.

Generator selection should ideally be based on a complete knowledge of all cost components. Variable and fuel cost are known for a unit MWh output, but not so the fixed capital, maintenance and transmission cost, which are only known for unit kW of capacity. Pre-run fixed cost per unit MWh cannot be determined because, at any hour during the simulation period, neither optimal generator locations, capacities, and transmission lines connecting them, nor the total annual output of these generators are known, since this requires knowledge of the system over the entire time period (the "pre-run fixed cost" problem). In order to be able to consider full cost per unit MWh at every hourly bidding step, we base our generator selection on data for variable cost plus *estimates* for fixed capital, maintenance and transmission cost. At the end of one simulation run, the generators selected in isolation for each hour are then compared and ranked based on their cost efficiency over the entire period, and uneconomic generators excluded. Runs are repeated, successively excluding generators, until a spatial optimum is achieved. The following sections describe this stepped, iterative procedure in further detail.

A.1.2 Resource potential and demand

The potential electrical energy PT_g^{et} generated by existing or proposed plants of nameplate capacity CP_g^e using energy carrier e at location g is

$$PT_g^{et} = CP_g^e + ST_g^{et} \ , \qquad \text{(A1.6)}$$

where ST_g^{et} is the storage capacity of those plants at time t. Data on the fuel type, geographical location and capacity of existing and proposed plant were sourced from Orr and Skeers 2014, with rooftop PV data available from APVI 2014.

For hypothetical plants from renewable sources such as wind or solar energy, the potential generation is calculated differently. For wind energy converters, we use

$$PT_g^{\mathrm{wind},t} = \rho_g^{\mathrm{wind},t}\eta^{\mathrm{wind}}\alpha^{\mathrm{wind}} = f\left(v_g^t\right)\eta^{\mathrm{wind}}\frac{\lambda^{\mathrm{wind}}\,\Delta a}{\rho^{\mathrm{wind}}(25\mathrm{ms}^{-1})}\,, \qquad \text{(A1.7)}$$

where $\rho_g^{\mathrm{wind},t} = f(v_g^t)$ is the wind power density as a near-cubic polynomial function f of wind speed v_g^t (Elliott *et al.* 1986), involving a cut-in speed of 4 ms^{-1} and a cut-out speed of 25 ms^{-1}, and scaled with a conversion efficiency of $\eta^{\mathrm{wind}} = 40\%$ (RAE 2014, Fig. A3a). The factor $\alpha^{\mathrm{wind}} = \lambda^{\mathrm{wind}}\,\Delta\mathrm{a}\,/\rho^{\mathrm{wind}}(25\mathrm{ms}^{-1}) = 1.6\,\mathrm{km}^2$ is a measure of maximum blade area per grid box, used to convert the wind power density into maximum available wind power. Here, $\lambda^{\mathrm{wind}} = 5\,\mathrm{MWkm}^{-2}$ is the wind capacity density limit (Short *et al.* 2011, p. 11; compare with 4 MWkm^{-2} assumed by Hoogwijk *et al.* 2004), Δa = 38.6km×38.6km is the area of one grid box, and $\rho^{\mathrm{wind}}(25\mathrm{ms}^{-1})$ is the maximum wind power density at 25 ms^{-1} cut-out speed. Gridded data on wind speed v_g^t were sourced from Huang 2014 (Figs. A4 and A5; hourly values were extracted as the minimum of pairs of half-hourly values).

For solar photovoltaic (PV) utilities we use

$$PT_g^{\mathrm{PV},t} = \left(\rho_g^{\mathrm{solar},t} - \theta^{\mathrm{PV}}\right)\eta^{\mathrm{PV}}\alpha^{\mathrm{PV}} = \rho_g^{\mathrm{solar},t}\eta^{\mathrm{PV}}\frac{\lambda^{\mathrm{PV}}\,\Delta a}{\rho^{\mathrm{max,solar}}}\,, \qquad \text{(A1.8)}$$

where $\rho_g^{\mathrm{solar},t}$ is the solar power density on the tilted surface, θ^{PV}= 120 Wm^{-2} is the irradiation threshold defined by the WMO 2003, $\eta^{\mathrm{PV}} = 15\%$ is the module efficiency, and the factor $\alpha^{\mathrm{PV}} = \lambda^{\mathrm{PV}}\,\Delta a\,/\rho^{\mathrm{max,solar}} = 4\,\mathrm{km}^2$ is a measure of maximum module area per grid box, used to convert the solar power density into maximum available PV power. Here, $\lambda^{\mathrm{PV}} = 48\,\mathrm{MWkm}^{-2}$ is the PV capacity density limit (Lopez *et al.* 2012, p. 3), and $\rho^{\mathrm{max,solar}} \approx 1200\,\mathrm{Wm}^{-2}$ is the maximum solar power density.

For concentrating solar power (CSP) we use

$$PT_g^{\mathrm{CSP},t} = \left(\rho_g^{\mathrm{solar},t} - \theta^{\mathrm{CSP}}\right)\eta^{\mathrm{CSP}}\alpha^{\mathrm{CSP}} = \left(\rho_g^{\mathrm{solar},t} - \theta^{\mathrm{CSP}}\right)\eta^{\mathrm{CSP}}\frac{\lambda^{\mathrm{CSP}}\Delta a}{\mu^{\mathrm{CSP}}\rho^{\mathrm{max,solar}}}, \qquad \text{(A1.9)}$$

where θ^{CSP}= 200 Wm^{-2} is the minimum solar power density to cover parasitic energy flows within the plant (IEA 2010, see Fig. A3b), $\eta^{\mathrm{CSP}} = 30\%$ is the CSP plant efficiency (Lovegrove *et al.* 2012, p. 49), and the factor $\alpha^{\mathrm{CSP}} = \left(\lambda^{\mathrm{CSP}}/\mu^{\mathrm{CSP}}\right)\Delta a\,/\rho^{\mathrm{max,solar}} = 2.6\,\mathrm{km}^2$ is a measure of maximum mirror area per grid box, used to convert the solar power density into maximum available CSP power. Here, $\lambda^{\mathrm{CSP}} = 62\ \mathrm{MWkm}^{-2}$ is the CSP capacity density limit, and $\mu^{\mathrm{CSP}} = 2/2.5$ is the solar multiple for plants with 5/15h of thermal storage (Gary *et al.* 2010; Turchi 2010; Short *et al.* 2011; IRENA 2012b; Jorgenson *et al.* 2013).

For PV and CSP, incident power density was computed as a function of surface tilt angle, latitude and longitude (Gilman 2014), air mass (Meinel and Meinel 1976; Kasten and Young 1989), and using a sun position algorithm (Reda and Andreas 2003). In essence, we take gridded data on air-mass-adjusted solar downwelling DW_{ij}^t (global horizontal irradiance) and the beam irradiance fraction FB_{ij}^t sourced from Huang 2014 (Figs. A4 and A5; hourly values were extracted as the minimum of pairs of half-hourly values), and calculate the direct normal irradiance beam as $DNI_g^t = \frac{DW_g^t FB_g^t}{\cos\left(Z_g^t\right)}$, where Z_g^t is the zenith angle. In a second step we calculate the beam irradiance incident on the tilted surface (plane-of-array irradiance) as $BI_g^t = DNI_g^t \cos\left(\theta_g^t\right)$, where θ_g^t is the solar incidence angle (Gilman 2014). With diffuse irradiance being $DI_g^t = DW_g^t(1 - FB_g^t)$, available solar power density is then $\rho_g^{\mathrm{solar},t} = BI_g^t + DI_g^t$. Self- and near-object shading was incorporated by setting the effective irradiance to 0 for zenith angles exceeding 80°. System losses such as soiling were considered as 11.3% of generation (Tab. 3 in Dobos 2014, excluding shading).

Not the entire resource potential is available for electricity generation. First, we excluded national parks and areas allowed for sustainable non-industrial use only (IUCN 2014; IUCN and UNEP 2014) as generator sites. Second, we excluded urban areas (ABS 2013) for CSP and wind power. Gridded geographical data on land area, national parks (IUCN categories I – V), sustainable use area (IUCN category VI), and urban land use faction were available from the IUCN World Database on Protected Areas IUCN and UNEP 2014 and Huang 2014, respectively (Fig. A5). Population data from the Australian Bureau of Statistics' Census (ABS 2013) were used to compute population density per square kilometre, which were then resampled to grid resolution. Hourly electricity demand data were taken from AEMO 2014a. Since such data were unavailable for Western Australia and the Northern Territory, the latter regions were approximated by data from South Australia, by scaling to adjust for population size and time zone.

A.1.3 Transmission

Spatial grid data on the existing transmission network capacity was constructed on the basis of network maps and information about the capacity (in units of MVA; AEMO 2010) of transmission lines run at different voltages (in units of kV; WALIA 2010; AEMO 2012; PowerWater 2014). As in AEMO 2013 (p. 80), additional transmission lines for the network expansion required to integrate yet unconnected dispersed solar and wind generators were constructed on the basis of information on the power flow between pairwise generators and consumers, gathered throughout each competitive selection run in form of a sparse tensor $F_g^{e,d}$ describing the flow of electricity generated by generator {*e*,*g*} using energy carrier *e* to consumer *d*. We first constructed transmission buses from locations with top-ranking generation values to the existing network, and then linked remaining locations as branches to these buses. Throughout the network expansion simulation, all additional lines were placed using link distance functions, thus ensuring connections with minimum distance and cost.

We calculated the cost CT_l of additional transmission at point l as $CT_l = \pi_k(k_l)\sqrt{\Delta a}$, where $\pi_k(k_l)$ the specific cost of a unit length of transmission line with a rated power capacity k_l (\$/km; data taken from AEMO 2012, see Fig. A10), k_l is the line capacity required in grid box *l*, and $\sqrt{\Delta a}$ is the linear size of a grid box. Total cost were allocated to generators on the basis of information participation of generators {*e*,*g*} in the capacity usage of transmission line segments located at *l*, gathered throughout each competitive selection run in form of a sparse line usage tensor $LU_g^{e,l}$. We assume that lines are overbuilt by 25% to handle contingency events (Section 6.3 in Short *et al.* 2011). We normalise the transmission line usage tensor to obtain a measure of line participation by generators {*e*,*g*}, as $LP_g^{e,l} = LU_g^{e,l} / \sum_{e,g} LU_g^{e,l}$.[1] Transmission cost CT_g^e allocated to generator {*e*,*g*} are then

$$CT_g^e = \sum_l LP_g^{e,l} \pi_k(k_l)\sqrt{\Delta a} \ . \qquad \text{(A.10)}$$

Distribution losses were estimated at 5.3% of demand (Section 3.1 in Short *et al.* 2011).

[1] Since total cost as a sum $\sum_l CT_l$ over line segments *l* must equal total cost as a sum $\sum_{e,g} CT_g^e$ over energy carriers and generators, we find $\sum_{e,g} CT_g^e = \sum_{e,g,l} LP_g^{e,l} \pi_k(k_l)\sqrt{\Delta a} = \sum_l \pi_k(k_l)\sqrt{\Delta a} \sum_{e,g} LP_g^{e,l} = \sum_l \pi_k(k_l)\sqrt{\Delta a} = \sum_l CT_l$,which yields the normalisation condition $\sum_{e,g} LP_g^{e,l} = 1 \forall l$. The line participation measure $LP_g^{e,l} = LU_g^{e,l} / \sum_{e,g} LU_g^{e,l}$ satisfies this normalisation condition.

A.2 Semi-formal description of the dispatch model used in this work

We emulate a competitive bidding process based on data on variable and fuel cost plus pre-run estimates of fixed capital, maintenance and transmission cost (because of the "pre-run fixed cost" problem explained earlier), with estimates adjusted after each run over the modelling period. This process progresses through four steps: We

a) carry out a time-sequential supply-demand matching run over the entire modelling period, using an initial estimate for technology-specific spot market offers calculated from fixed and variable cost (Tab. 1), calculate post-run capital and operational cost per unit of electricity output for every generator, and, at the end of the period:
b) extend the existing transmission network as required to connect all unconnected generators, and calculate additional transmission cost per unit of electricity output for every generator,
c) exclude generators starting with those of highest total cost per unit of output, until the sum of excluded output equals the reliability standard for maximum unserved energy (0.002% of total demand),
d) start a new run, with the spot market offers adjusted to the technology-specific total cost per unit of output obtained in the previous run.

Thus, an increasing number of uneconomic sites are being excluded in successive runs, leading to an overall decrease in system cost, until a local optimum for the spatial generator configuration is reached.

In each optimisation run, our dispatch model proceeds as follows (a more formal and exhaustive exposition can be found in Lenzen *et al.* 2015):

1. Initialise capacity CP_g^e (APVI 2014; Orr and Skeers 2014), output OU_g^{et} (zero array), and cost variables (Tab. 1) for t = 0.

2. Sequentially loop through the time period [0,T].
   2.1 Read demand $DM^{d,t}$ at time t for all demand locations, and add a contingency and frequency regulation reserve of 15% (compare p. 33 and Tab. 11 in Short *et al.* 2011, and p. 101 in AEMO 2013).
   2.2 Randomly loop through all demand locations d.
   2.2.1 Establish the Euclidean distance ED_g^d between demand location d and generator locations g.
   2.2.2 Estimate relative transmission and distribution loss TL_g^d = (1 – $6.25\times10^{-5}\ ED_g^d$) × (1 – 5.3%) between location d and all other grid points (Short *et al.* 2011, p. 30, transmission losses are assumed 1%/100 miles).
   2.2.3 Construct a *pre-run estimate* (denoted by a tilde (~) accent, see the pre-run fixed cost problem described in the main text) for unit transmission cost for an electricity bundle $DM^{d,t}$ as $\widetilde{CT}_g^d = \left[(m + \chi_{1i} + \chi_{1s})DM^{d,t} + y_0)ED_g^d\right]\frac{(1+\chi_2)(1+\delta\iota)}{LT^eKF_g^e}$, where m = 3.4417×10^{-4} \$m/km/MW and y_0 = 0.3644 \$m/km are the regression constants in Fig. A10, χ_{1i} = \$0.234m/MW are interconnect cost (Short *et al.* 2011,

Tab. 7; assumed to apply for any 1000km length), χ_{1s} = \$0.024m/MW are substation and transformer costs (Short *et al.* 2011, Tab. 7; assumed to apply for any 100km length, see AEMO 2011, Tab. 8-1[2]), $\chi_2 = 25\%$ is the transmission contingency factor (Short *et al.* 2011, Section 6.2), ι = 8% and δ = 50% are interest rate and debt fraction (Short *et al.* 2011, Tab. 9), and LT^e and KF_g^e hold technology-specific plant lifetimes and capacity factors, respectively (Tab. 1). Note this estimate is arrived at without knowledge of the post-run spatial configuration of generators. Transmission cost are therefore re-calculated after having iterated through the period T.

2.2.4 Similarly, construct a *pre-run estimate* for fixed capital and maintenance cost, as $\widetilde{CC}_g^e + \widetilde{CF}_g^e = (CC^e + CF^e)\frac{(1+\delta\iota)}{LT^e KF_g^e}$. Fixed costs are also re-calculated after having iterated through the period T.

2.2.5 Set bid $BD_g^{e,d}$ offered by generators {*e*,*g*} as the sum of unit-output capital cost ($\widetilde{CC}$), fixed and variable operating and maintenance cost ($\widetilde{CF}$ and CV), fuel cost (CL) as well as a transmission cost estimate ($\widetilde{CT}$), initially as $BD_g^{e,d} = \widetilde{CC}_g^e + \widetilde{CF}_g^e + CV^e + CL^e + \widetilde{CT}_g^d$.

2.2.6 Successively accept lowest bids until $DM^{d,t}$ is satisfied.

3. Construct transmission network to link up participating generators.
   3.1 Calculate post-run additional transmission cost CT_g^d applying data shown in Tab. A10 to the network just constructed.
   3.2 Exclude generators starting with those of highest total cost per unit of output, until the sum of excluded output equals the reliability standard for maximum unserved energy (0.002% of total demand over period T, see Section 4.2 in AEMO 2013).
   3.3 Update capacity CP_g^e.
   3.4 Go to step 2.

In principle, a selection order can be established based on the cost data shown in Tab. 1 (see Tab. A3). Strictly following step 2.2.5 means that a less expensive technology would be exclusively selected over any more expensive technology, even if cost differences were minimal. Given that in any case cost characteristics will vary amongst plants, we apply a random term to all cost terms $C \in \{\widetilde{CC}, \widetilde{CF}, CV, CL\}$, and substitute $C_g^e \to C_g^e + |R_g^e(CoV^e)|$, where $R_g^e(CoV^e)$ is a normally distributed random variable over the simulation grid with standard deviation CoV^e specific to technologies e (Tab. 1). This randomisation of cost washes out the strict selection thresholds in step 2.2.5, and leads to a broader range of technologies being selected in any one scenario.

[2] The value in Short *et al.* 2011, Tab. 7 (\$24/kW) is of the same order of magnitude as an estimate derived from AEMO 2011 Tab. 8-1 (\$30m/(2 ×1245 MVA) ≈ \$12/kW).

A.3 Figures illustrating data underlying our simulation

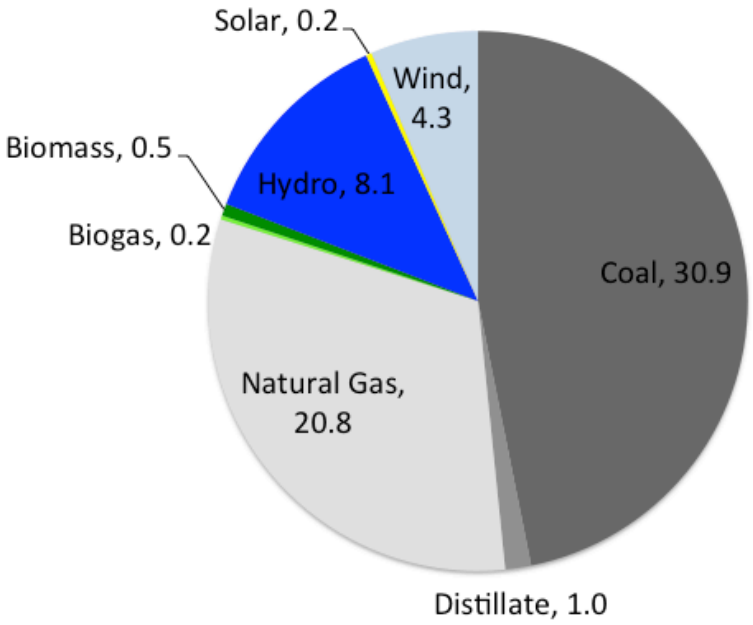

Fig. A1: Utility-scale generation capacity installed in Australia's NEM as of 2014 (in units of GW, total = 66 GW, based on data in Orr and Skeers 2014).

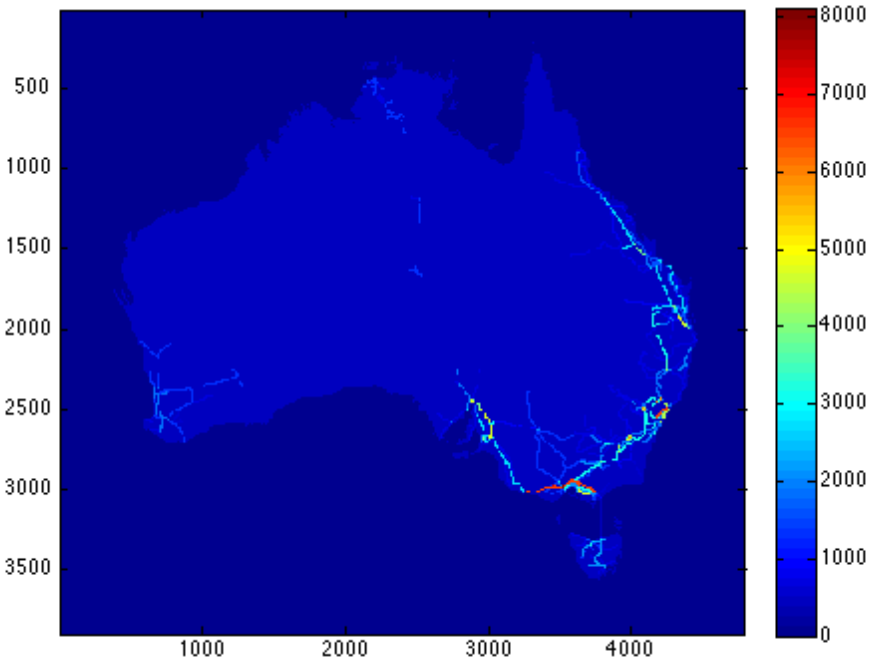

Fig. A2: Transmission network capacity (converted from voltage in kV into capacity in MVA; AEMO 2010; WALIA 2010; AEMO 2012; PowerWater 2014). Axes in km.

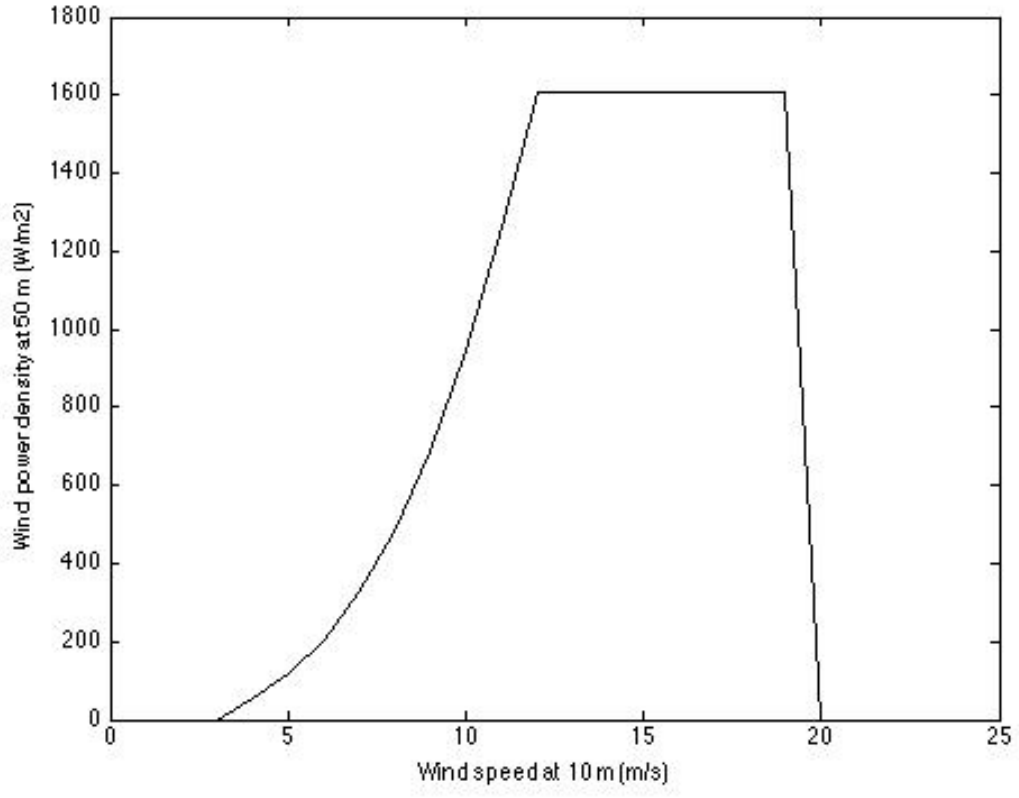

Fig. A3a: Wind power density at 50 m height as a function $f\left(v_{ij}^{t}\right)\eta^{\text{wind}}$ of wind speed v_{ij}^{t} at 10 m height, for conversion efficiency $\eta^{\text{wind}} = 40\%$ (RAE 2014).

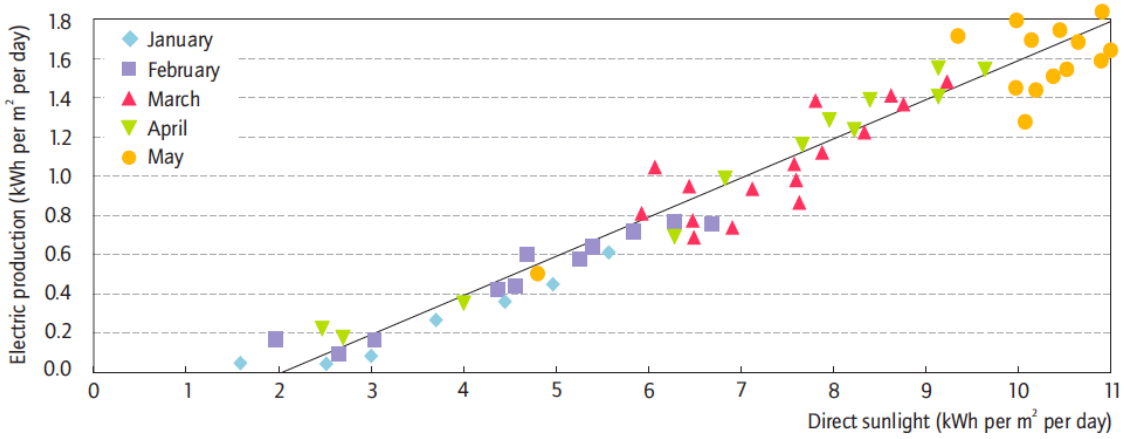

Fig. A3b: Electricity output as a function of insolation, yielding a conversion efficiency $\eta^{\text{CST}} = 20\%$ and an operation threshold of 2 kWh $m^{-2}d^{-1} \approx 200$ Wm^{-2} (Fig. 1 from IEA 2010).

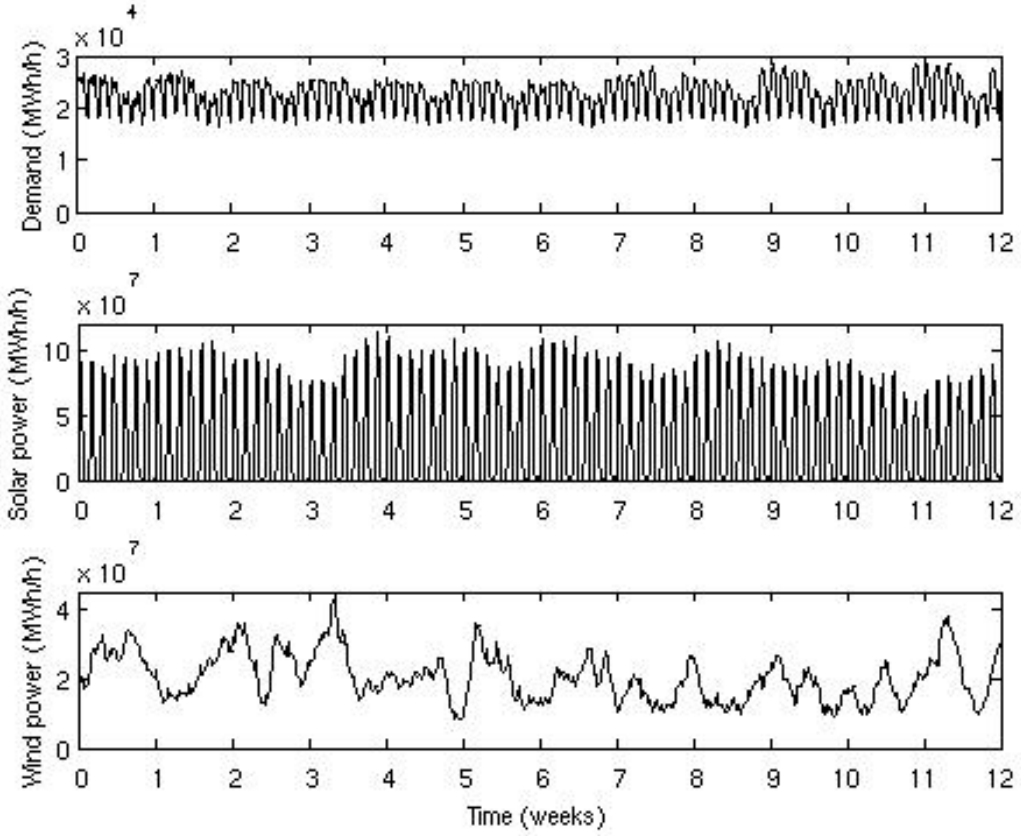

Fig. A4: Electricity demand, wind power $\sum_g PT_g^{\mathrm{wind},t}$ and solar power $\frac{1}{2}\left(\sum_g PT_g^{\mathrm{PV},t} + \sum_g PT_g^{\mathrm{CSP},t}\right)$ across Australia for a twelve-week period 1 October – 23 December 2010.

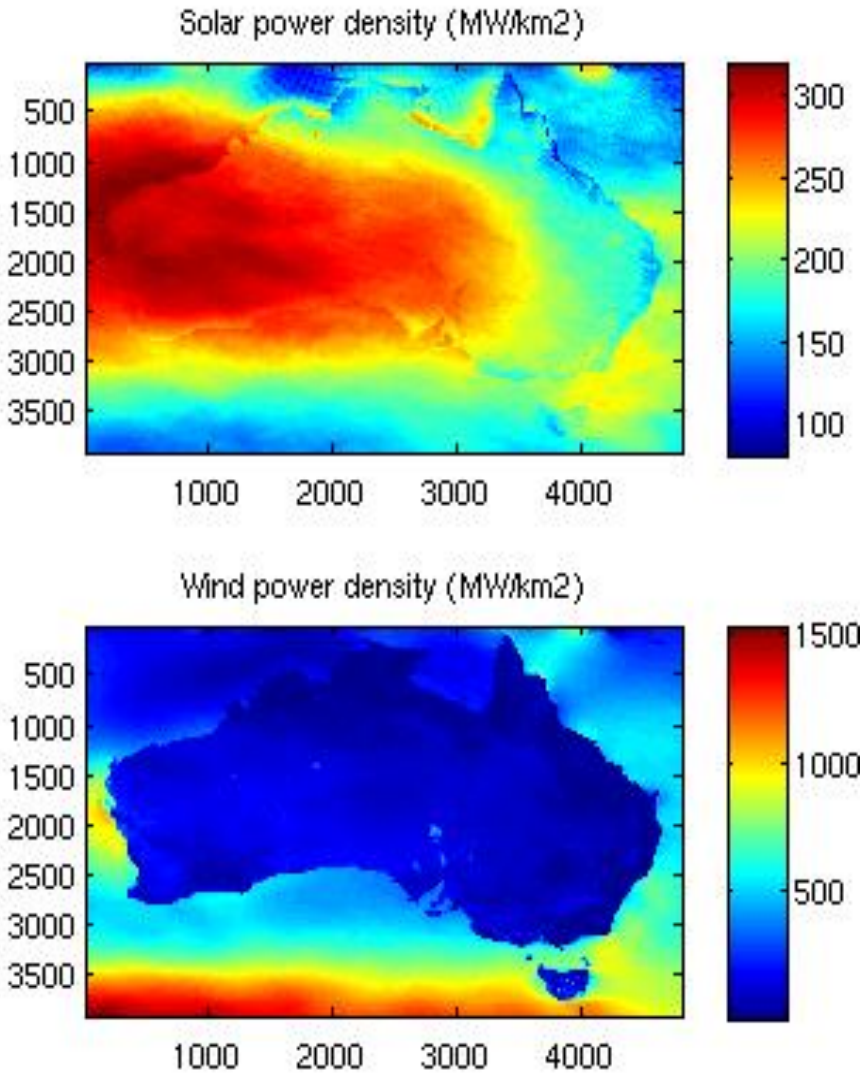

Fig. A5: Average wind power density $\overline{\rho_{ij}^{\text{wind}}}$ and solar power density $\overline{\rho_{ij}^{\text{solar}}}$ across Australia for a twelve-week period 1 October – 23 December 2010. Axes in km.

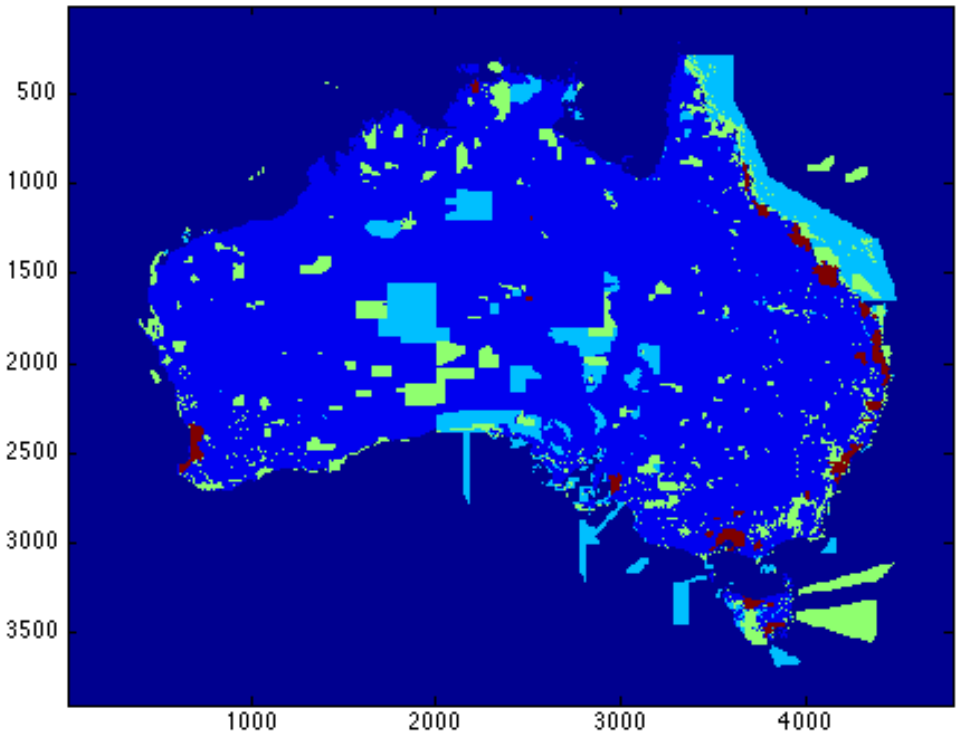

Fig. A6: Populated areas (red), national parks (IUCN categories I-V, green; IUCN and UNEP 2014) and areas for sustainable use (IUCN category VI, light blue; IUCN 2014). Axes in km.

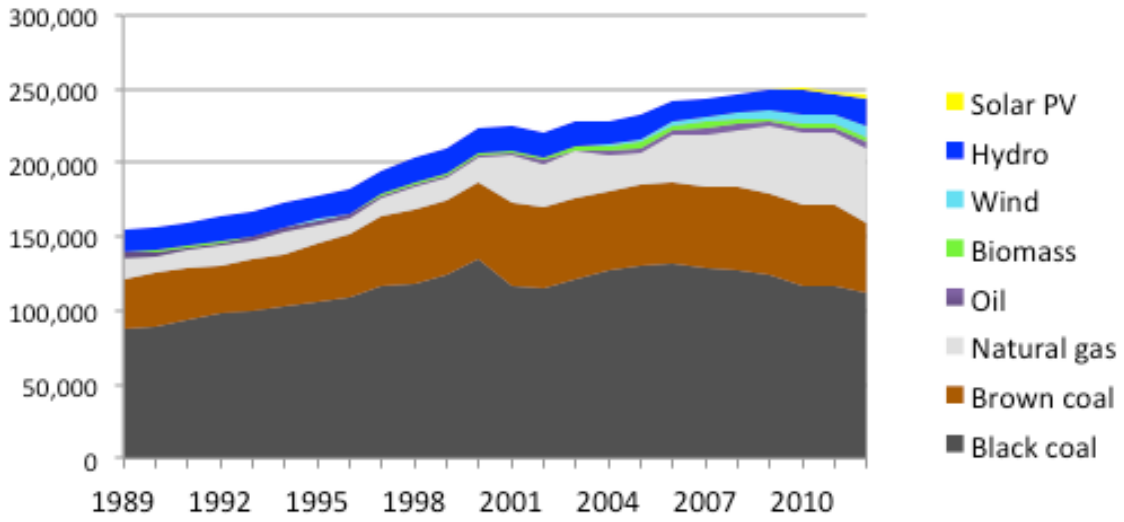

Fig. A7: Electricity generation (in units of GWh) by fuel in Australia 1989-2014.

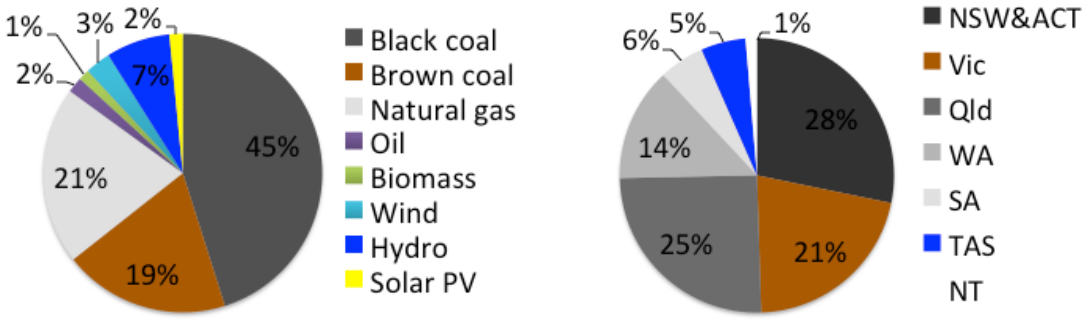

Fig. A8: Electricity generation (in percentages) by fuel and by State and Territory in Australia in 2013 (BREE 2013).

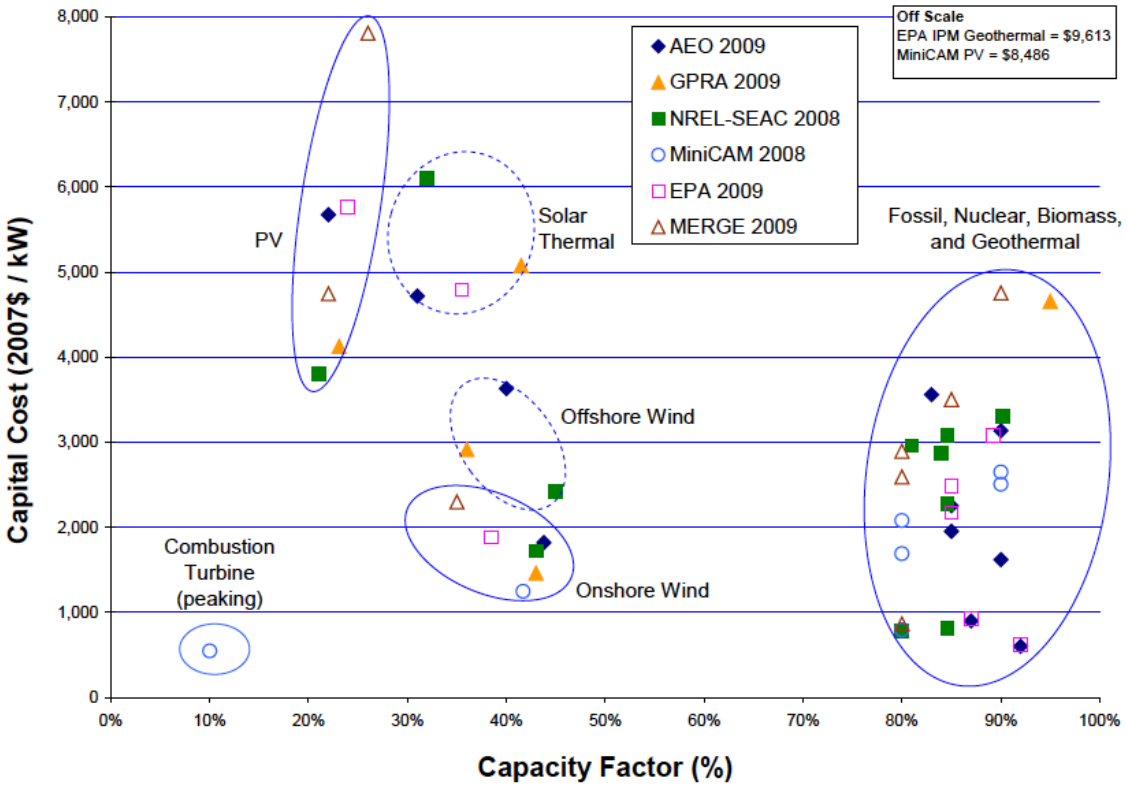

Figure 22. Overnight capital costs versus capacity factors, 2010

Fig. A9: Capital cost comparison between technologies (taken from Tidball *et al.* 2010).

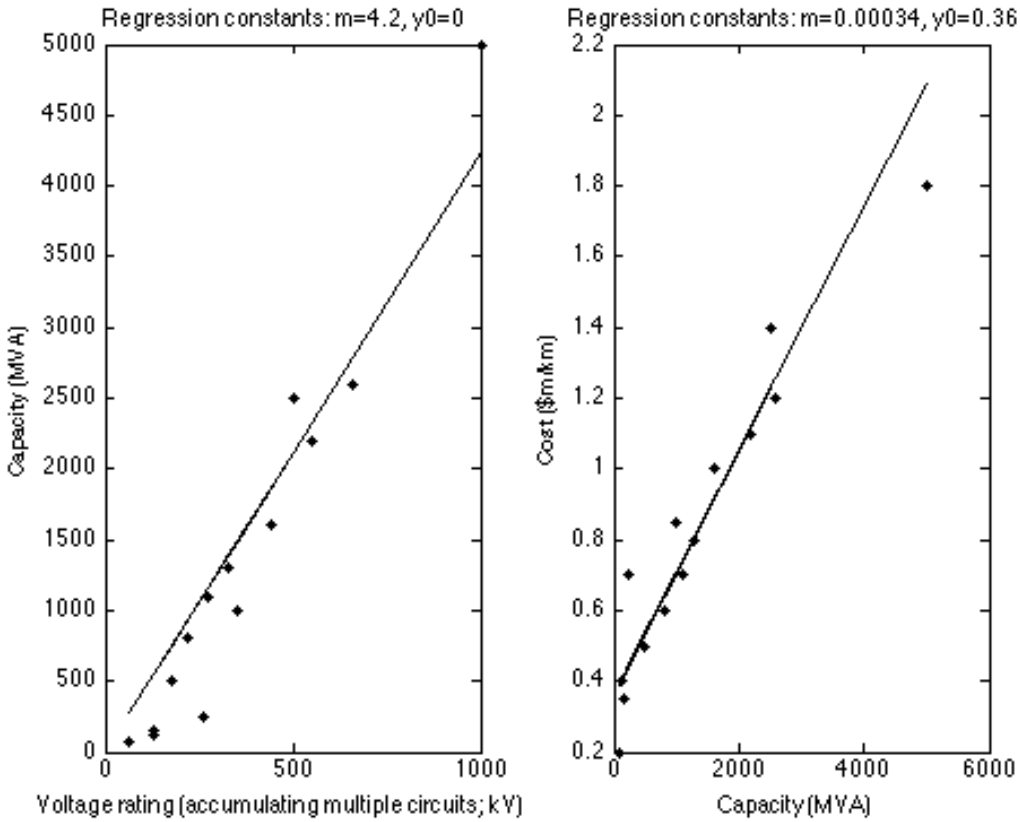

Fig. A10: Regression of transmission capacity (in units of MVA; accumulated over multiple circuits) as a function of voltage rating (in kV; left panel) and transmission cost (in $m/km) as a function of transmission capacity (in MVA; right panel), derived from data in AEMO 2012.

A.4 Detailed review of technology cost

Energy carrier	Capital cost ($/kW)	Fixed operation & maintenance cost ($/MW/y)	Variable operation & maintenance cost ($/MWh generated)	Reference	Comments
Coal					
	3124	60,500	8	AETA 2013	Pulverised coal
	3246	37,800	4.47	EIA	
	2890	23,000	4	NREL 2010	2010 PC
	2890	23,000	4	NREL 2010	2050 PC
Gas					
	1062	10,000	4	AETA 2013	CCGST
	1230	6,020	4	NREL 2010	2010
	1230	6,000	4	NREL 2010	2050
Wind					
	2530	40,000	12	AETA 2013	
	2579			AEMO 2013	
	2678	35,000	10.5	AEMO 2013	2030 scenario 1
	1764	50,607	19	AEMO 2013	2030 scenario 2
	2600	30,000	9	AEMO 2013	2050 scenario 1
	1813	58.207	17.5	AEMO 2013	2050 scenario 2
	1938-2145			EPA 2011	
	2213	39,550		EIA 2013	
	1800-2200			IRENA 2012b	
	1980	59,000		NREL 2010	2010
	1980	59,000		NREL 2010	2050

Tab. A1: Cost estimates for various electricity-generating technologies.

Energy carrier	Capital cost ($/kW)	Fixed operation & maintenance cost ($/MW/y)	Variable operation & maintenance cost ($/MWh generated)	Reference	Comments
PV Utility					
	3380	30,000-40,000	25	AETA 2013	
	3822			AETA 2013	
	1228	33,250		AEMO 2013	2030 scenario 1
	2160	48,077		AEMO 2013	2030 scenario 2
	1584	28,500		AEMO 2013	2050 scenario 1
	1544	57,279		AEMO 2013	2050 scenario 2
	3350			Feldman *et al.* 2014	
	3873	24,690		EIA 2013	
	4978-9322			EPA 2011	
	8000-10000			Tidball *et al.* 2010	
	4000	50,000		NREL 2010	2010
	2030	30,000		NREL 2010	2050
CSP					
	8950	65,000	20	AETA 2013	Parabolic trough, 6 hr storage
	8308	60,000	15	AETA 2013	Central receiver, 6 hr storage
	8282			AEMO 2013	
	4642	52,500	13.1	AEMO 2013	2030 scenario 1
	5514	75,911	19	AEMO 2013	2030 scenario 2
	3811	45,000	11.3	AEMO 2013	2050 scenario 1
	4414	87,311	21.8	AEMO 2013	2050 scenario 2
	6500			Feldman *et al.* 2014	
	5067	67,260		EIA 2013	
	2024-6071			Turchi 2010 Hinkley *et al.* 2011	Data by Hinkley refers to solar towers
	7100-9800			IRENA 2012b	6 hr storage
	6300-10500			IRENA 2012b	6-15 hr storage
	7060	50,000		NREL 2010	2010

Tab. A1: Cost estimates for various electricity-generating technologies (cont.).

Energy carrier	Capital cost ($/kW)	Fixed operation & maintenance cost ($/MW/y)	Variable operation & maintenance cost ($/MWh generated)	Reference	Comments
Hydro	4700	50,000		NREL 2010	2050
	3936	14,130		EIA 2013	
	1050-7650			IRENA 2012a	
	3500-5500	15,000	16	NREL 2010	2010
Pumped Hydro					
	4487			AEMO 2013	
	4487	48,999	6.7	AEMO 2013	2030 scenario 1
	4487	70,848	9.7	AEMO 2013	2030 scenario 2
	4487	41,999	5.8	AEMO 2013	2050 scenario 1
	4487	81,488	11.2	AEMO 2013	2050 scenario 2
	5288			EPA 2011	
Biomass					
	5000	125,000	8	AETA 2013	
	5123			AEMO 2013	
	4700	109,375	7	AEMO 2013	2030 scenario 1
	5220	158,148	10.1	AEMO 2013	2030 scenario 2
	5527	93,750	6	AEMO 2013	2050 scenario 1
	5325	181,896	11.6	AEMO 2013	2050 scenario 2
	8180	356,070	17.49	EIA 2013	Circulating Fluidised Bed
	4114	105,630	5.26	EIA 2013	Bubbling Fluidised Bed
	1880 – 6800			IRENA 2012a	Co-fired
	3830	94,000	15	NREL 2010	2010
	3830	94,000	15	NREL 2010	2050

Tab. A1: Cost estimates for various electricity-generating technologies (cont.).

Energy carrier	Capital cost ($/kW)	Fixed operation & maintenance cost ($/MW/y)	Variable operation & maintenance cost ($/MWh generated)	Reference	Comments
Wave					
	5900	190,000		AETA 2013	
	2511	166,250		AEMO 2013	2030 scenario 1
	3671	240,384		AEMO 2013	2030 scenario 2
	2465	142,500		AEMO 2013	2050 scenario 1
	3521	276,484		AEMO 2013	2050 scenario 2
Geothermal					
	10600	170,000		AETA 2013	Dry rock
	7920			AEMO 2013	2030 Hot Dry Rock scenario 1
	10634			AEMO 2013	2030 Hot dry rock scenario 2
	5230	175,000		AEMO 2013	2030 Aquafier Scenario 1
	7064	253,036		AEMO 2013	2030 Aquafier Scenario 2
	7946	150,000		AEMO 2013	2050 scenario 1
	10815	291,036		AEMO 2013	2050 scenario 2

Tab. A1: Cost estimates for various electricity-generating technologies (cont.).

	Scenario 1	Scenario 2
Transformation of the electricity sector	rapid	moderate
Economic and electricity and demand growth	moderate	robust
Demand side participation	strong	weak

Tab. A2: Definition of scenarios in AEMO 2013.

	Carbon price ($/t)															
Bidding rank	0	10	20	30	40	50	60	70	80	90	100	110	120	130	140	150
1	Gas	Gas	Gas	Hydro	Hydro	Hydro	Hydro	Hydro	Hydro	Hydro	Hydro	Hydro	Hydro	Hydro	Hydro	Hydro
2	Coal	Hydro	Hydro	Gas	Gas	Biomass	Biomass	Biomass	Biomass	Biomass	Biomass	Biomass	Biomass	Biomass	Biomass	Biomass
3	Hydro	Coal	Biomass	Biomass	Biomass	Gas	Utility PV	Utility PV	Utility PV	Utility PV	Utility PV	Utility PV	Utility PV	Utility PV	Utility PV	Utility PV
4	Biomass	Biomass	Coal	Utility PV	Utility PV	Utility PV	Ocean	Ocean	Ocean	Ocean	Ocean	Ocean	Ocean	Ocean	Ocean	Ocean
5	Utility PV	Utility PV	Utility PV	Ocean	Ocean	Ocean	Gas	Wind	Wind	Wind	Wind	Wind	Wind	Wind	Wind	Wind
6	Ocean	Ocean	Ocean	Wind	Wind	Wind	Wind	Gas	Gas	Geoth	Geoth	Geoth	Geoth	Geoth	Geoth	Geoth
7	Wind	Wind	Wind	Coal	Geoth	Geoth	Geoth	Geoth	Geoth	CSP 15h	CSP 15h	CSP 15h	CSP 15h	CSP 15h	CSP 15h	CSP 15h
8	Geoth	Geoth	Geoth	Geoth	Coal	CSP 15h	CSP 15h	CSP 15h	CSP 15h	Gas	Gas	CSP 5h	CSP 5h	CSP 5h	CSP 5h	CSP 5h
9	CSP 15h	CSP 15h	CSP 15h	CSP 15h	CSP 15h	Coal	CSP 5h	CSP 5h	CSP 5h	CSP 5h	CSP 5h	Gas	Gas	Gas	CSP no st	CSP no st
10	CSP 5h	CSP 5h	CSP 5h	CSP 5h	CSP 5h	CSP 5h	Coal	Coal	CSP no st	CSP no st	CSP no st	CSP no st	CSP no st	CSP no st	Gas	Gas
11	CSP no st	CSP no st	CSP no st	CSP no st	CSP no st	CSP no st	CSP no st	CSP no st	Coal	Coal	Coal	Coal	Coal	Coal	Coal	Coal

Technology	**Total cost ($/MWh)**															
Coal	25.5	35.5	45.5	55.5	65.5	75.5	85.5	95.5	105.5	115.5	125.5	135.5	145.5	155.5	165.5	175.5
Gas	9.0	15.7	22.3	29.0	35.7	42.3	49.0	55.7	62.3	69.0	75.7	82.3	89.0	95.7	102.3	109.0
Biomass	38.3	38.3	38.3	38.3	38.3	38.3	38.3	38.3	38.3	38.3	38.3	38.3	38.3	38.3	38.3	38.3
Hydro	26.2	26.2	26.2	26.2	26.2	26.2	26.2	26.2	26.2	26.2	26.2	26.2	26.2	26.2	26.2	26.2
Utility PV	45.5	45.5	45.5	45.5	45.5	45.5	45.5	45.5	45.5	45.5	45.5	45.5	45.5	45.5	45.5	45.5
Wind	52.5	52.5	52.5	52.5	52.5	52.5	52.5	52.5	52.5	52.5	52.5	52.5	52.5	52.5	52.5	52.5
CSP no st	95.8	95.8	95.8	95.8	95.8	95.8	95.8	95.8	95.8	95.8	95.8	95.8	95.8	95.8	95.8	95.8
CSP 5h st	81.5	81.5	81.5	81.5	81.5	81.5	81.5	81.5	81.5	81.5	81.5	81.5	81.5	81.5	81.5	81.5
CSP 15h st	67.2	67.2	67.2	67.2	67.2	67.2	67.2	67.2	67.2	67.2	67.2	67.2	67.2	67.2	67.2	67.2
Rooftop PV																
Ocean	46.4	46.4	46.4	46.4	46.4	46.4	46.4	46.4	46.4	46.4	46.4	46.4	46.4	46.4	46.4	46.4
Geoth	63.3	63.3	63.3	63.3	63.3	63.3	63.3	63.3	63.3	63.3	63.3	63.3	63.3	63.3	63.3	63.3

Tab. A3: Bidding rank order under various carbon price assumptions.

Energy carrier	PV	CSP	Bio	Wd	PV	CSP	Bio	Wd	PV	CSP	Bio	Wd
{φ, ψ, ϕ, ω}	l	h	l	l	h	h	l	l	h	l	l	l
Total cost ($/MWh)	67	82	29	49	111	82	29	49	111	49	29	49
Rank	3	4	1	2	4	3	1	2	4	2	1	2
Energy carrier	PV	CSP	Bio	Wd	PV	CSP	Bio	Wd	PV	CSP	Bio	Wd
{φ, ψ, ϕ, ω}	l	h	h	l	a	a	a	a	h	l	l	h
Total cost ($/MWh)	67	82	48	49	89	66	38	65	111	49	29	81
Rank	3	4	1	2	4	3	1	2	4	2	1	3
Energy carrier	PV	CSP	Bio	Wd	PV	CSP	Bio	Wd	PV	CSP	Bio	Wd
{φ, ψ, ϕ, ω}	l	h	h	h	l	l	h	h	h	l	h	h
Total cost ($/MWh)	67	82	48	81	67	49	48	81	111	49	48	81
Rank	2	4	1	3	3	2	1	4	4	2	1	3

Tab. A4: Bidding rank order for four renewable energy carriers at $1000/t carbon price and generation cost variations as in the 3×3 panels in Figs. A11-A18. 'Wd' = Wind, 'l' = low (cost multiplier 0.75), 'h' = high (cost multiplier 1.25). Total cost calculated as in Tab. 1, as {ϕ, ψ, φ, ω} × {[capital cost ×(1+$\delta\iota$)/(8760h/y × LT) + fixed O&M cost/8760h/y] / capacity factor + variable cost + fuel cost}, where LT is the plant lifetime, ι=8% is the assumed interest rate, and δ=50% is the debt fraction (Short et al. 2011, Tab. 9), but with capacity factors of utility PV and wind of 10% and 30%, respectively.

A.5 Additional detailed results

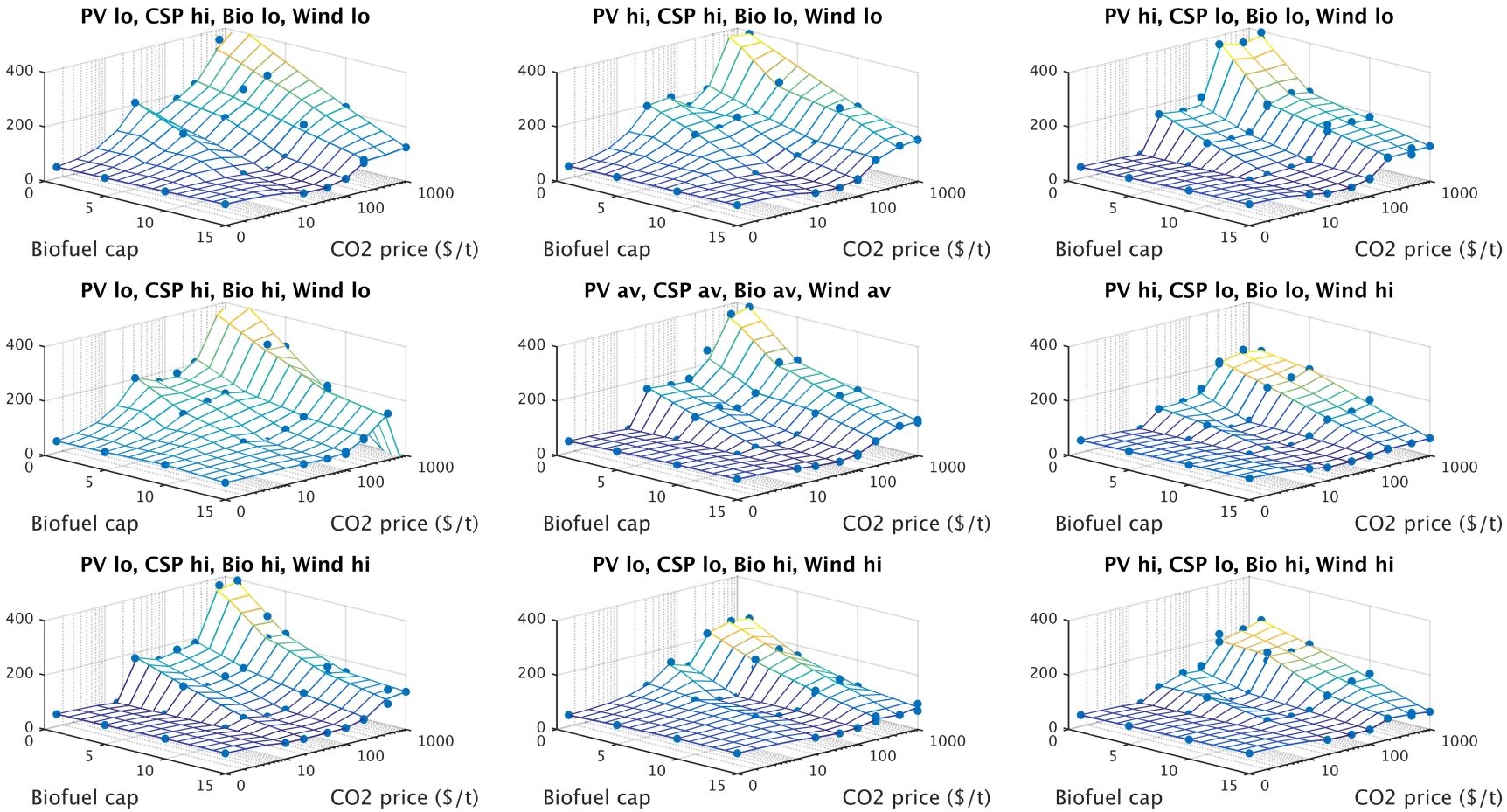

Fig. A11: As in Fig. 2, system-wide installed capacity in units of GW for runs parameterised by $1 \le \beta \le 15$ and $0 \le \kappa \le 1000$. The nine panels show interpolations from runs (blue dots) with varying cost multipliers 0.75 ("lo") $\le \{\phi, \psi, \varphi, \omega\} \le$ 1.25 ("hi"). $\{\phi, \psi, \varphi, \omega\} = 1$ is denoted "av". The results show that installed capacity increases with decreasing cost (and hence in our simulation increasing penetration) of technologies with low degrees of dispatchability, ie wind and PV. Installed capacity is highest for low PV and wind, and high CSP and biofuels cost (centre left panel), and lowest for high PV and wind, and low CSP and biofuels cost (centre right panel). All other cost combinations lead to intermediate results.

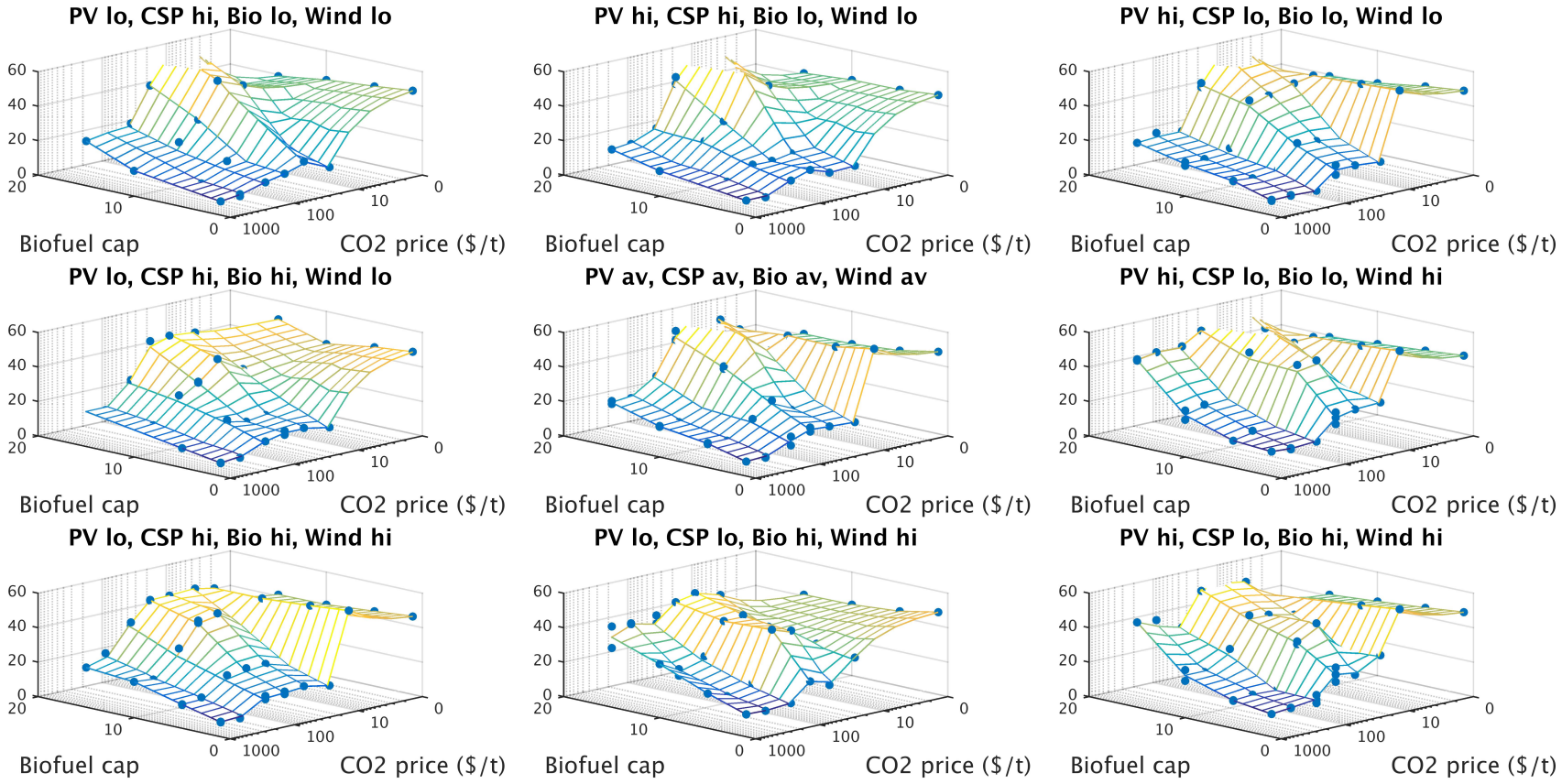

Fig. A12: As in Fig. 2, system-wide capacity factor (in %) for runs parameterised by $1 \le \beta \le 15$ and $0 \le \kappa \le 1000$. The nine panels show interpolations from runs (blue dots) with varying cost multipliers 0.75 ("lo") $\le \{\phi, \psi, \varphi, \omega\} \le$ 1.25 ("hi"). $\{\phi, \psi, \varphi, \omega\} = 1$ is denoted "av". The variation is not as pronounced as that of installed capacity, but effects can clearly be seen when viewing the surface point at $\beta = 15$ and $\kappa = 1000$. The results show that the capacity factor decreases with decreasing cost (and hence in our simulation increasing penetration) of technologies with low degrees of dispatchability, ie wind and PV. The capacity factor at $\kappa = 1000$ is lowest for low PV and wind, and high CSP and biofuels cost (centre left panel), and highest for high PV and wind, and low CSP and biofuels cost (centre right panel). All other cost combinations lead to intermediate results.

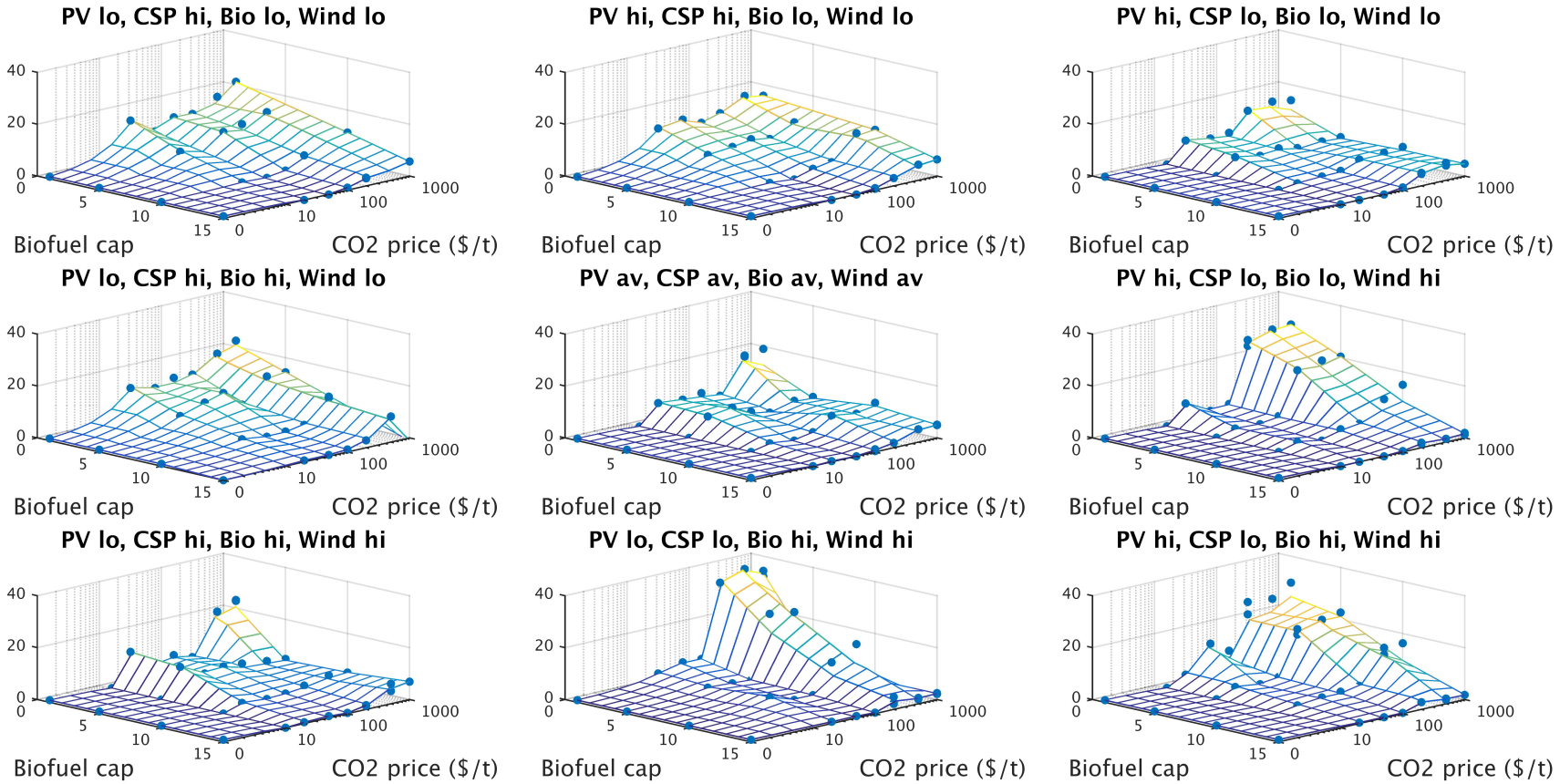

Fig. A13: As in Fig. 2, system-wide spilled energy as a percentage of total generation for runs parameterised by $1 \le \beta \le 15$ and $0 \le \kappa \le 1000$. The nine panels show interpolations from runs (blue dots) with varying cost multipliers 0.75 ("lo") $\le \{\phi, \psi, \varphi, \omega\} \le$ 1.25 ("hi"). $\{\phi, \psi, \varphi, \omega\} = 1$ is denoted "av". The variation is not as pronounced as that of installed capacity. Spilled energy appears highest when CSP cost are low compared to the default situation (see Tab 1). This is due to the circumstance that at low cost CSP replaces biofuels as the dominant energy source in renewables-only technology mixes (see Fig. A16). This is due to CSP's high capacity factor, however, its generation cost is still comparable with or higher than that of wind and PV, meaning that wind and PV capacities become more fully utilised, leading to relatively low spillage for wind and PV, and relatively high spillage for CSP.

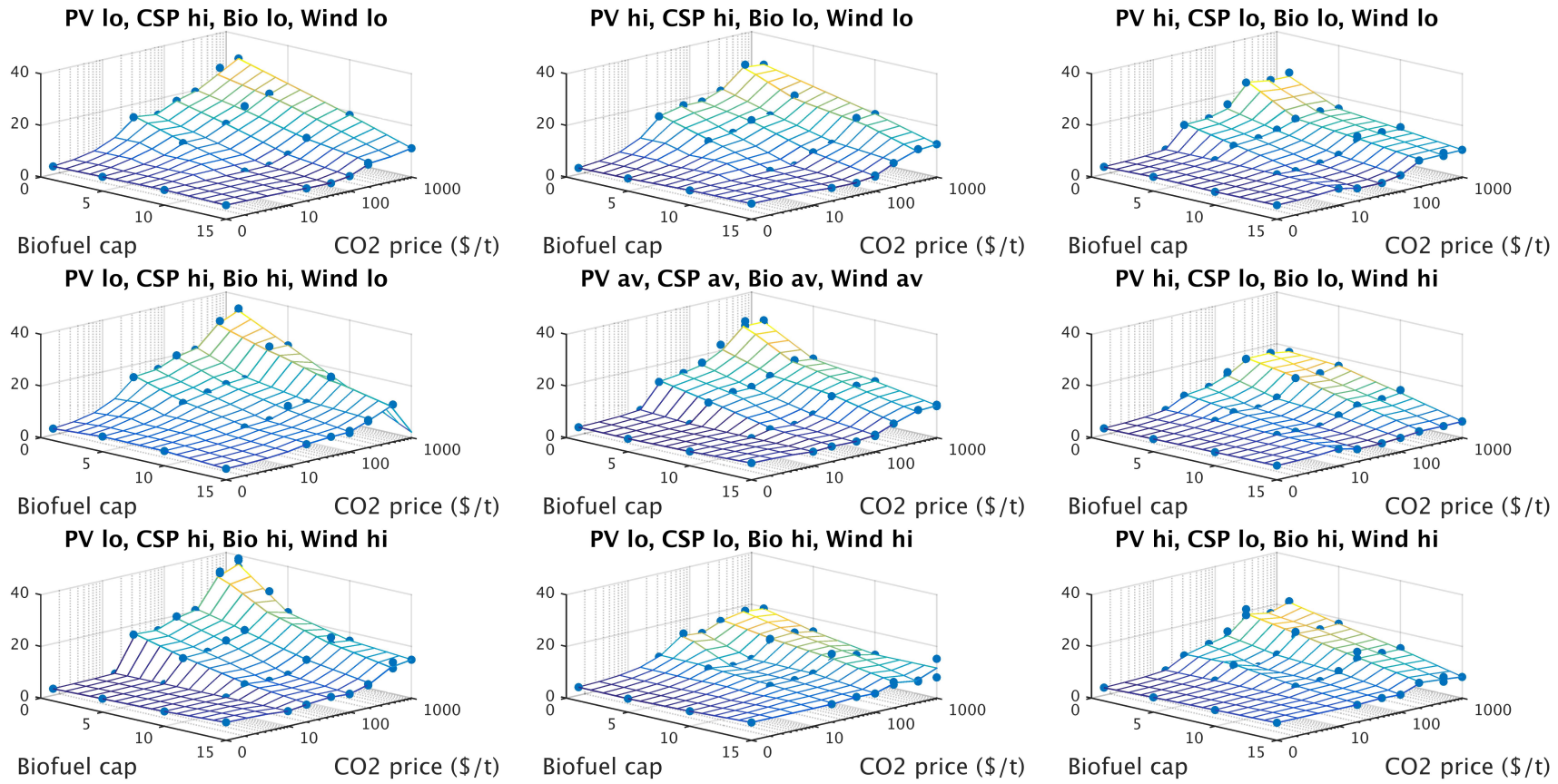

Fig. A14: As in Fig. 2, system-wide total cost in units of ¢/kWh for runs parameterised by $1 \le \beta \le 15$ and $0 \le \kappa \le 1000$. The nine panels show interpolations from runs (blue dots) with varying cost multipliers 0.75 ("lo") $\le \{\phi, \psi, \varphi, \omega\} \le$ 1.25 ("hi"). $\{\phi, \psi, \varphi, \omega\} = 1$ is denoted "av". The results are much in line with those for installed capacity, showing that total cost increase with decreasing cost (and hence in our simulation increasing penetration) of technologies with low degrees of dispatchability, ie wind and PV. Total cost are highest for low PV and wind, and high CSP and biofuels cost (centre left panel), and lowest for high PV and wind, and low CSP and biofuels cost (centre right panel). All other cost combinations lead to intermediate results.

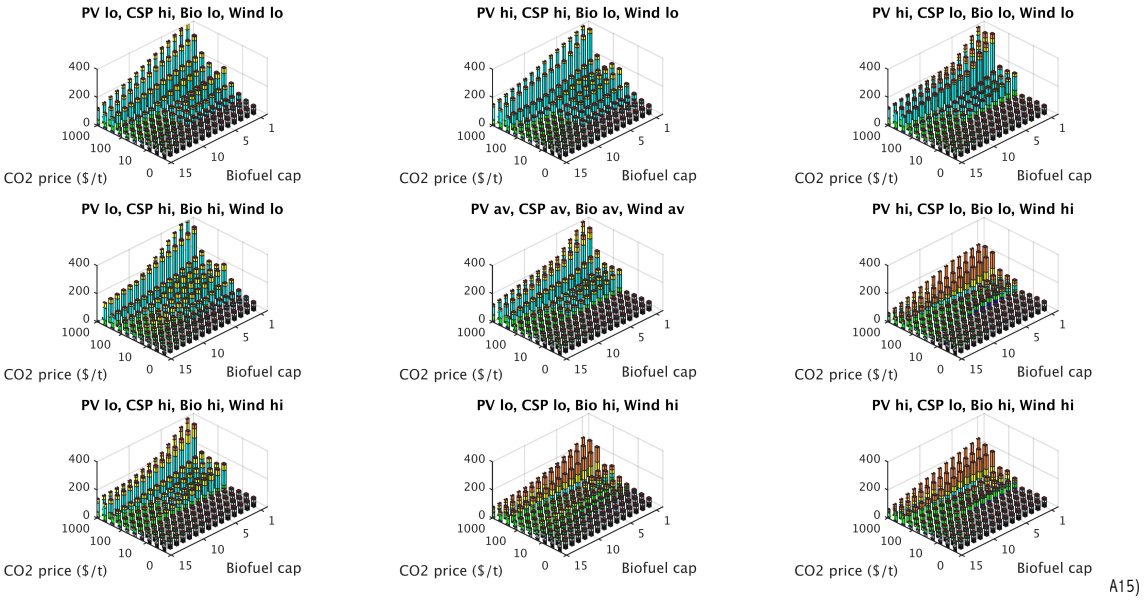

A15)

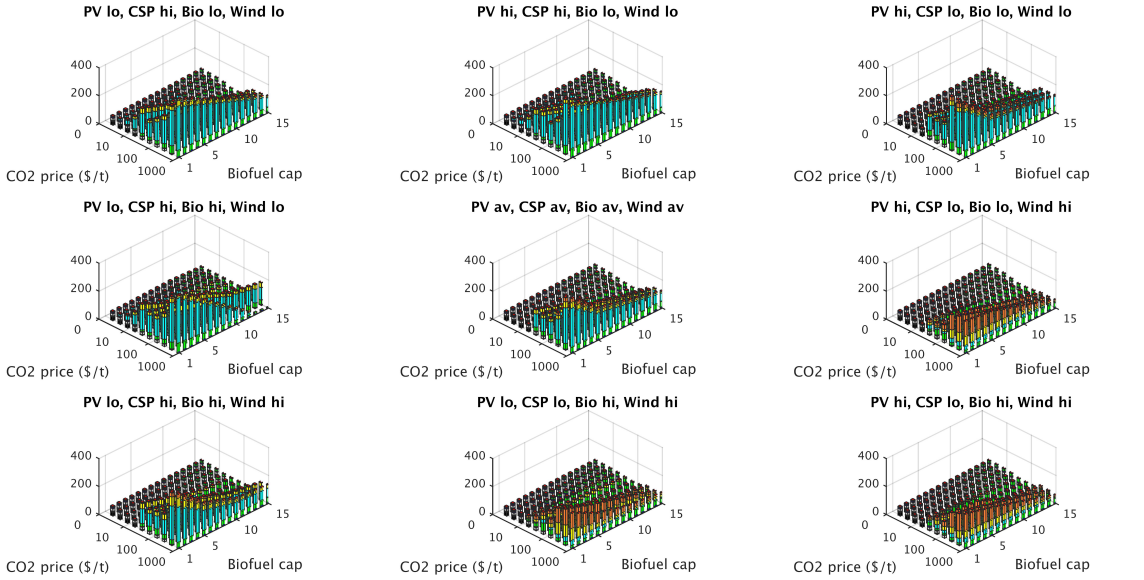

A16)

Figs. A15-A16: As in Fig. 3, system-wide technology mix in terms of installed capacity in units of GW for runs parameterised by $1 \le \beta \le 15$ and $0 \le \kappa \le 1000$. The nine panels show interpolations from runs with varying cost multipliers 0.75 ("lo") $\le \{\phi, \psi, \varphi, \omega\} \le 1.25$ ("hi"). $\{\phi, \psi, \varphi, \omega\} = 1$ is denoted "av". Front (a) and rear (b) views of the column landscape are shown for convenience. In addition to Fig. A11 the results show that at $\kappa = 1000$ wind and CSP dominate the capacity mix because these technologies feature both high penetration and relatively low systemic capacity factor. In addition, the technology mix is strongly influenced by the relative cost of wind. Wind installed capacity is high for low wind cost, and CSP installed capacity is high for high wind cost. All other cost combinations lead to intermediate results.

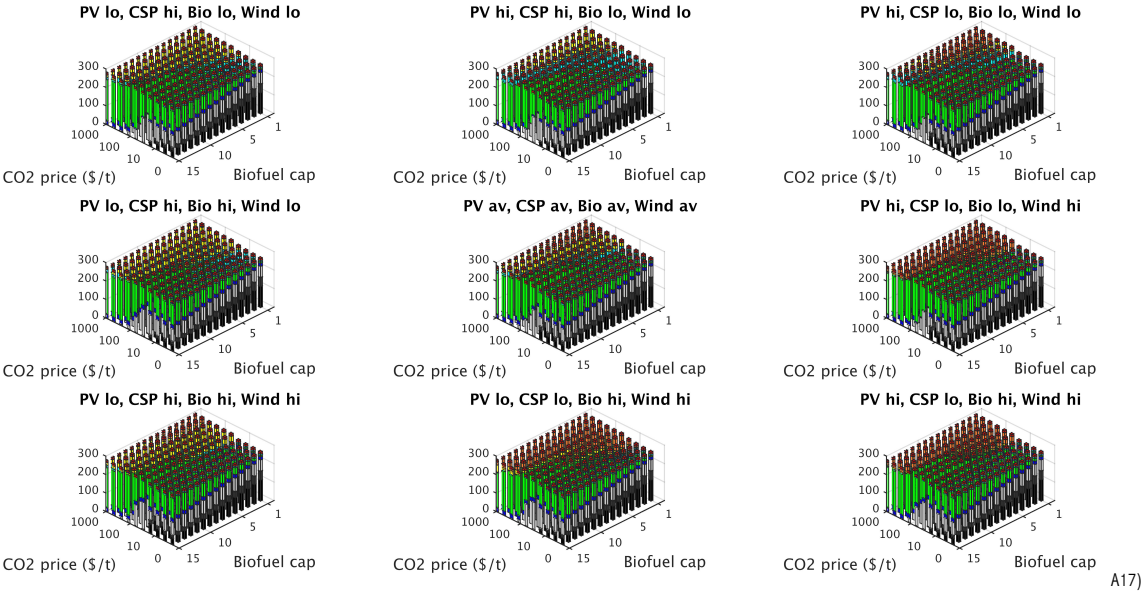

A17)

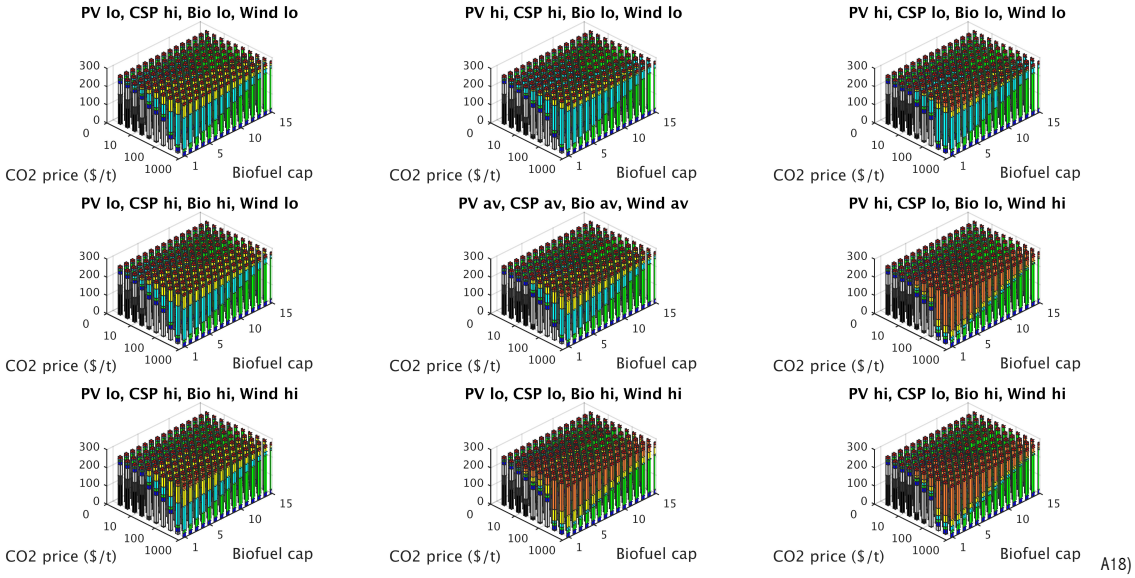

A18)

Figs. A17-A18: As in Fig. 3, system-wide technology mix in terms of generation in units of TWh for runs parameterised by $1 \le \beta \le 15$ and $0 \le \kappa \le 1000$. The nine panels show interpolations from runs with varying cost multipliers 0.75 ("lo") $\le \{\phi, \psi, \varphi, \omega\} \le$ 1.25 ("hi"). $\{\phi, \psi, \varphi, \omega\} = 1$ is denoted "av". Front (a) and rear (b) views of the column landscape are shown for convenience. In addition to Fig. A11 the results show that at $\kappa = 1000$, wind dominates when its cost are low (centre left panel), CSP dominates when its cost are low and wind cost are high (southeast panels), and PV achieves its highest penetration when its cost are low and all other cost are high (bottom left). All other cost combinations lead to intermediate results.

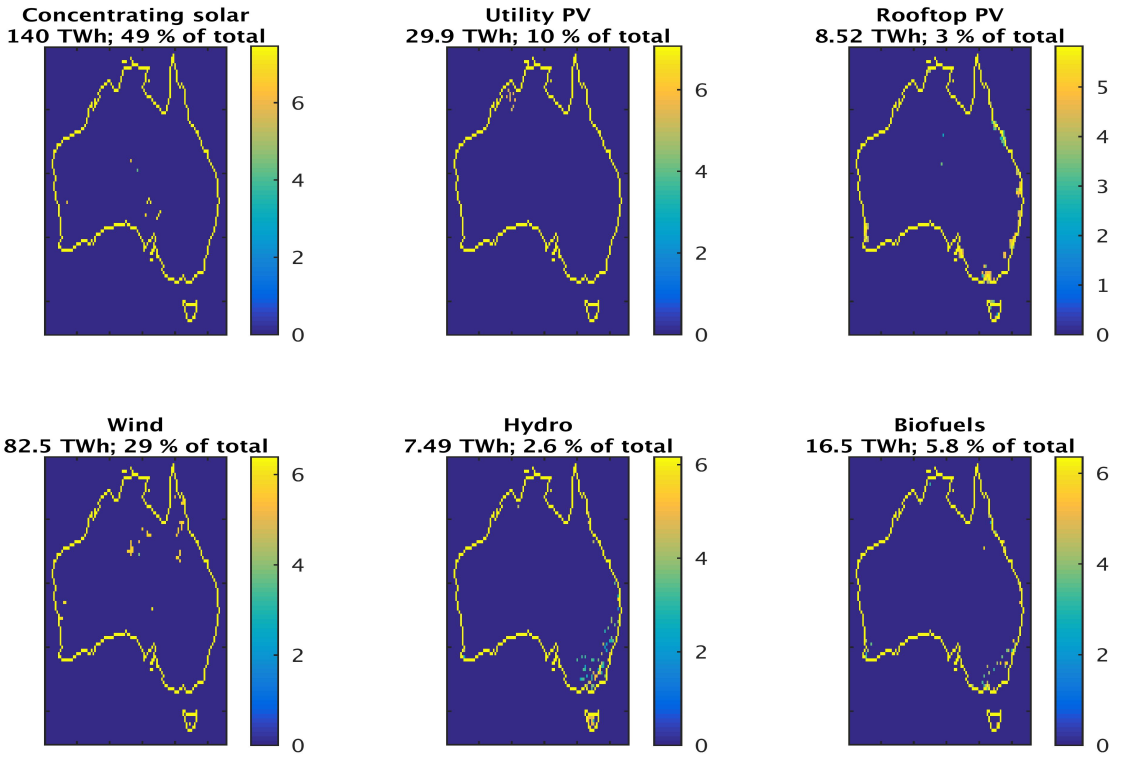

Fig. A19: Spatial and technology distribution of generation (in units of TWh) for a run with β = 15, κ = 1000 $/t, ϕ = 1.00, ψ = 0.85, φ = 4.10, ω = 1.10, and 15 h CSP storage. Concentrating solar located in the arid centre of Australia contributes almost 50% to generation, followed by wind (29%) and PV (10%). Hydro and biofuelled generation occurs at existing sites mainly in southeastern Australia, whilst rooftop PV is obviously restricted to urban areas. Note that wind penetration is below levels assumed to be problematic in terms of system integration[3], and biofuelled generation is below the 20 TWh assumed by Elliston *et al.* 2013.

[3] Voorspools and D'haeseleer 2006; Hoogwijk *et al.* 2007; Meibom *et al.* 2007; Holttinen 2008; Resch *et al.* 2008.

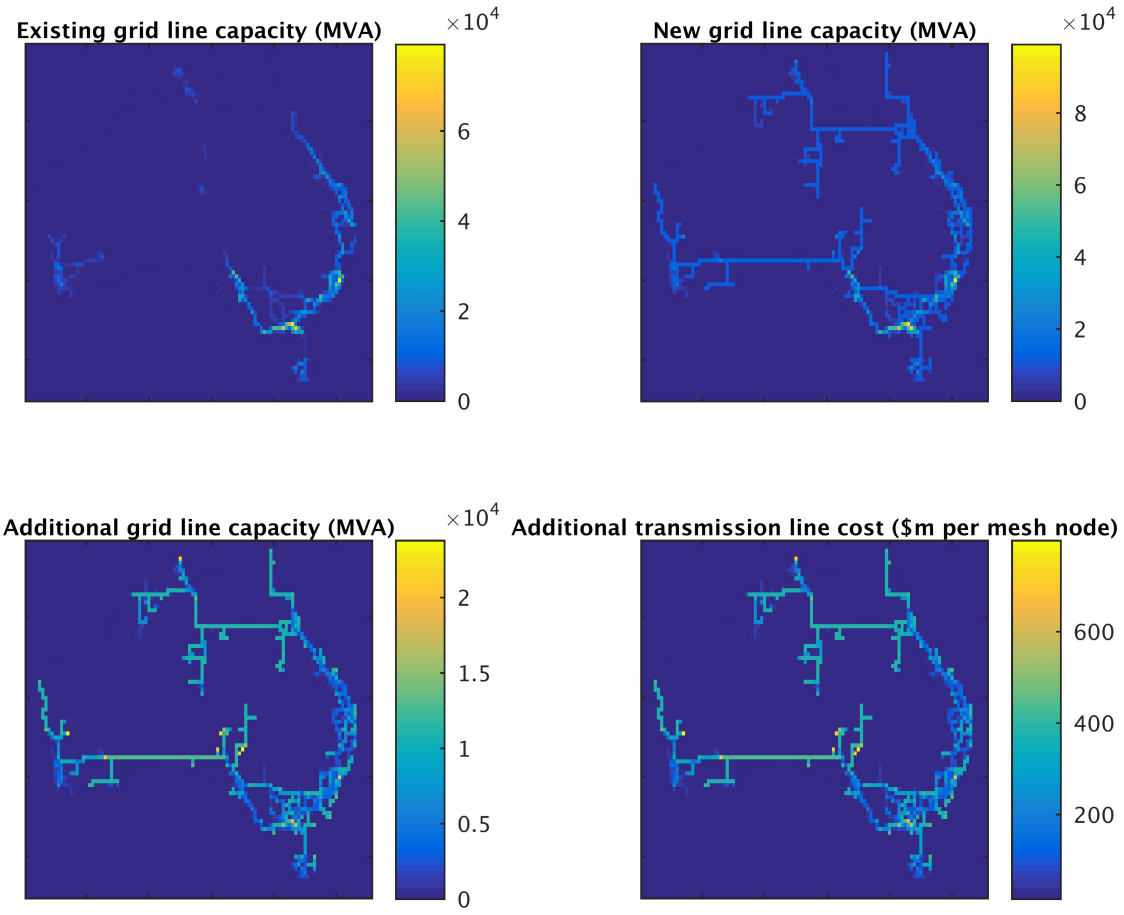

Fig. A20: Transmission network capacity (in units of MVA) and additional transmission line cost for a run with β = 15, κ = 1000 $/t, ϕ = 1.00, ψ = 0.85, φ = 4.10, ω = 1.10, and 15 h CSP storage. Given that a) transmission cost are lower than fixed cost on a per-kWh basis, b) transmission losses are relatively low at 1% per 100 miles (Short *et al.* 2011, p. 30), and c) generation is spatially dispersed in a renewables-only grid, we find that cross-continental links of the currently isolated network becomes beneficial.

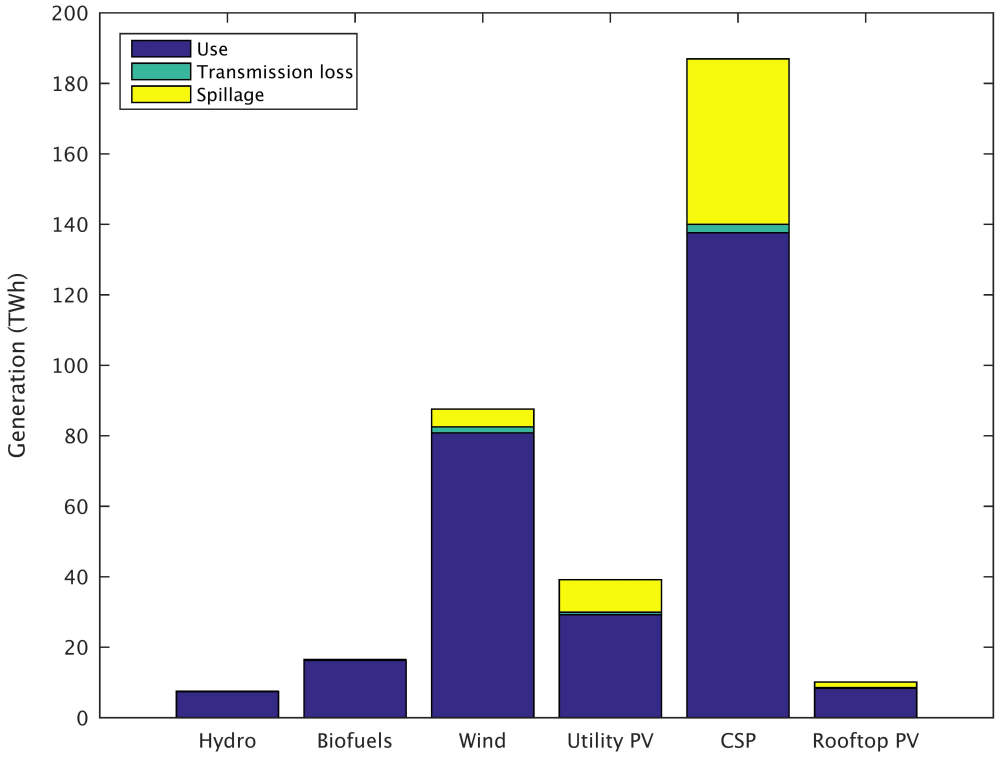

Fig. A21: Use, transmission loss, and spillage, by technology, in units of TWh for a run with β = 15, κ = 1000 $/t, ϕ = 1.00, ψ = 0.85, φ = 4.10, ω = 1.10, and 15 h CSP storage (compare Tab. 2).

A.6 Limitations because of spatial and temporal resolution of weather data

A.6.1 Irradiance data

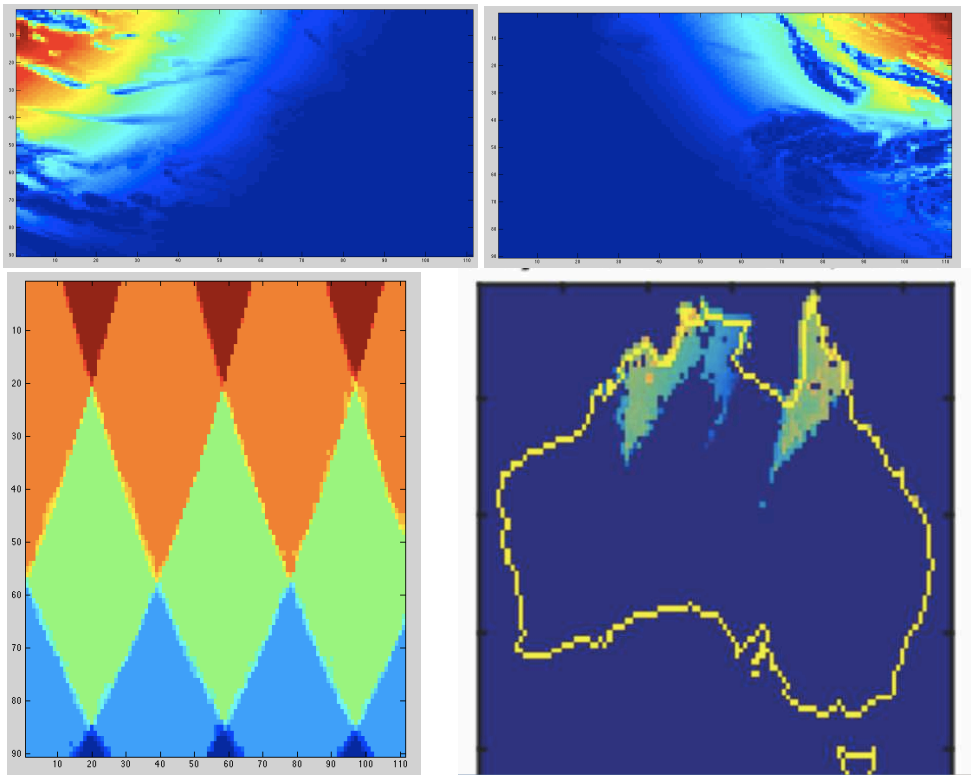

Fig. A22: The hourly temporal resolution of irradiance data creates discrete "fronts" delineating areas with and without sunshine (top panels). As these fronts traverse the continent in hourly steps, some areas (within a front) receive up to two hours more sunshine than areas directly adjacent (outside the front). This circumstance leads to a streaked pattern in the sunshine hours variable (bottom left panel). These streaks are at times imposed on the generator selection for utility PV plants (bottom right panel). CSP plants are unaffected because their selection is strongly influenced by the 15-hour storage capacity. Rooftop PV performance is also unaffected because this technology is spatially restricted to urban areas.

A.6.2 Wind data

The wind speed data (see Fig. A5 bottom panel) shows a marked increase at the continental coastline, with wind speeds being significantly higher off-shore. We conducted a numerical simulation where we increased the area permissible for generator locations by one grid cell around the entire continent, thus including an off-shore area of roughly 39 km distance. We observed a) an increased concentration of selected generator sites around the coastline at the cost of inland sites (Fig. A23), b) a decreased need for biofuels, concentrating solar, and hydropower to plug supply gaps created by the variability of wind energy (Fig. A24), and an increase of wind's capacity factor from 18% to 31%, as evident from the load duration curves (Fig. A25).

The increased capacity factor is in line with values reported by Elliston *et al.* 2013 (30%), but still not as high as those measured by {AEMO, 2014 #5733} and published by Miskelly 2012 (around 35%). The latter high capacity factors may be typical for isolated wind turbines and small wind farms, however recent studies report shading effects limiting the capacity factor of large wind farms to around 20% (see Fig. 1 in Miller *et al.* 2015[4]). Therefore, even though we do not explicitly model shading effects, our results may be realistic for situations of high wind energy penetration.

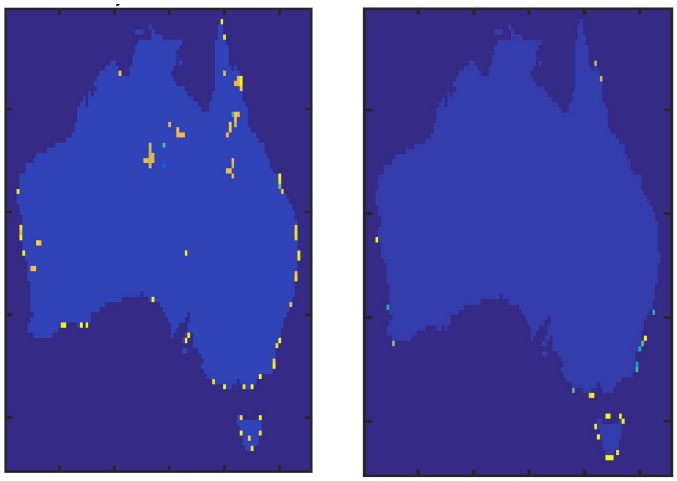

Fig. A23: Increased concentration of selected wind generators. Left panel: wind generator siting excluding a 39-km offshore strip (compare Fig. 4 in the main text); right panel: wind generator siting including a 39-km offshore strip.

[4] Based on Short *et al.* 2011 (p. 11) we assumed a wind capacity density limit of $\lambda^{\mathrm{wind}} = 5\ \mathrm{MWkm}^{-2}$. Miller *et al.* 2015 show that for this installed capacity density, delivered energy density will not exceed 1 MW km^{-2} (their Fig. 2, see also Adams and Keith 2013), and hence capacity factors will be limited to 20% (their Fig. 1, blue bar).

The increased capacity factor for offshore wind causes a decreased need for biofuels, concentrating solar, and hydropower to plug supply gaps created by the variability of wind energy. As a consequence, in the offshore scenario installed biofuelled capacity decreases to 3.8 GW, overall installed capacity decreases to 110 GW, the capacity factors of biofuels and concentrating solar increase to 39% and 44% respectively, and the system's overall capacity factor increases to 36%.

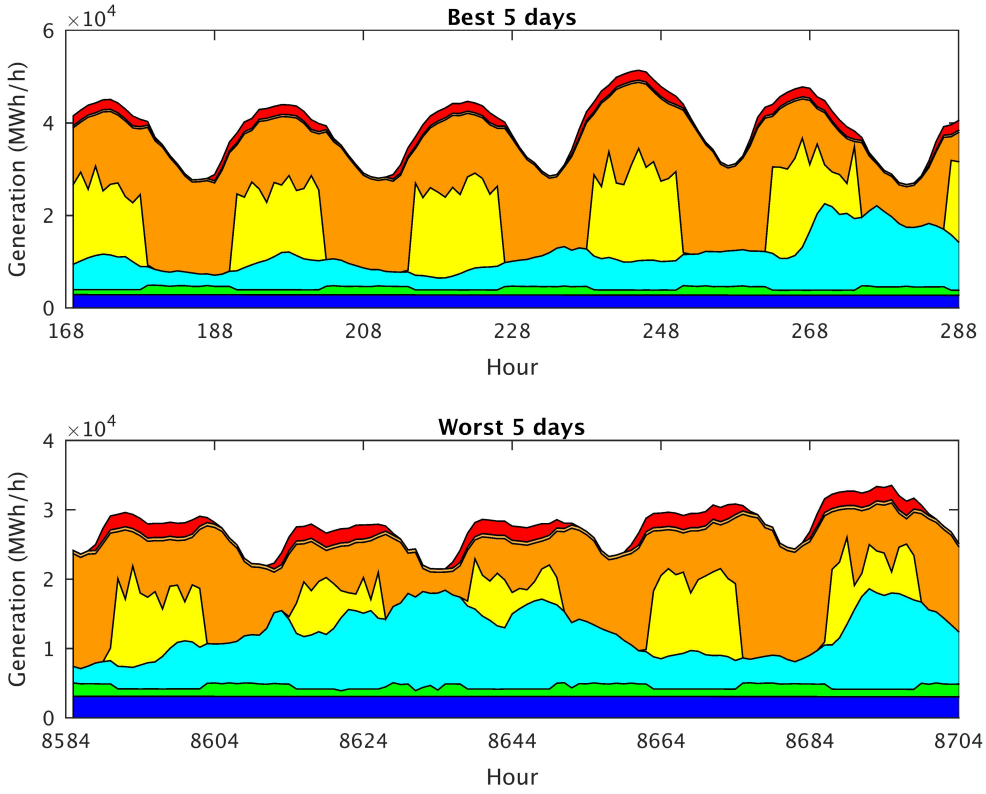

Fig. A24: 5-day generation profiles in a simulation including offshore area, for one period with minimum combined hydro and biofuelled generation ("best 5 days" in 2010 for renewables, beginning of January, top panel), and one period with the maximum combined hydro and biofuelled generation ("worst 5 days", mid-December, bottom panel). Dark blue: hydro, green: biofuels, light blue: wind, yellow: utility PV, orange: CSP, red: rooftop PV. The decreased variability and increased contribution of wind energy are clearly discernible (compare with Fig. 6 in the main text).

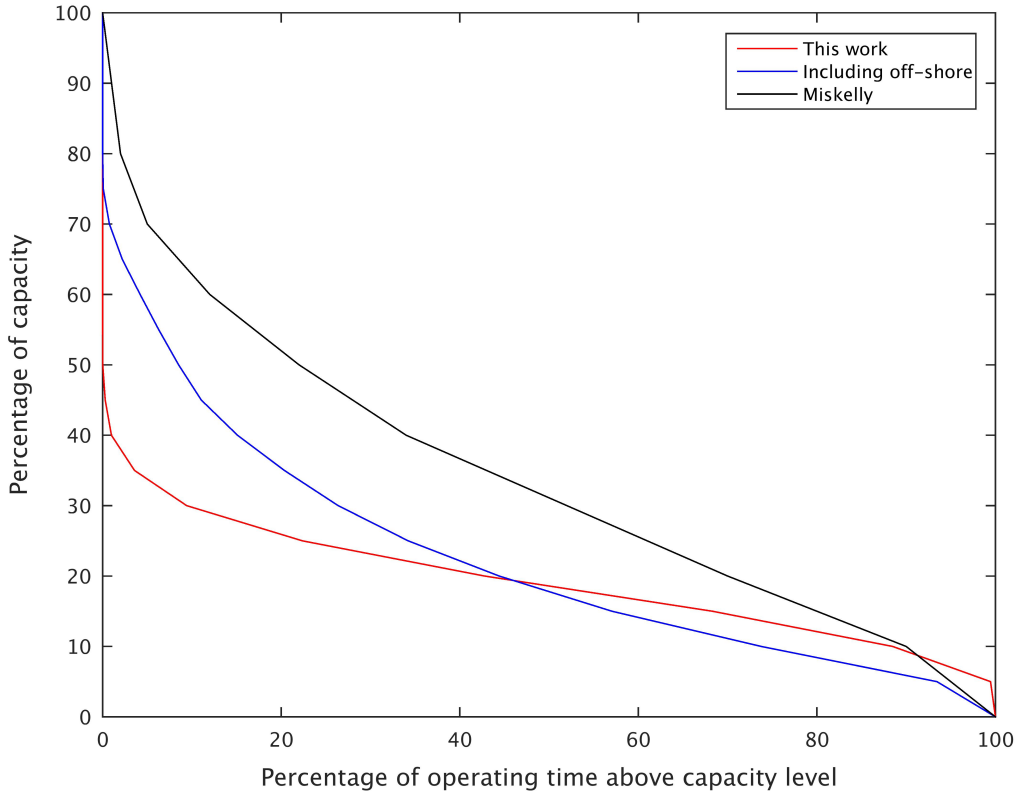

Fig. A25: A comparison of load duration curves (for dispatched and spilled energy) excluding off-shore areas (red, compare Fig. 5 in the main text), and including off-shore areas (blue), with measured South Australian load duration data (black) published by AEMO 2014b and Miskelly 2012. The latter high capacity factors may be typical for isolated wind turbines and small wind farms, however recent studies report shading effects limiting the capacity factor of large wind farms to around 20% (see Fig. 1 in Miller *et al.* 2015[5]). Therefore, even though we do not explicitly model shading effects, our results may be realistic for situations of high wind energy penetration.

[5] Based on Short *et al.* 2011 (p. 11) we assumed a wind capacity density limit of $\lambda^{\mathrm{wind}} = 5\ \mathrm{MWkm}^{-2}$. Miller *et al.* 2015 show that for this installed capacity density, delivered energy density will not exceed 1 MW km^{-2} (their Fig. 2, see also Adams and Keith 2013), and hence capacity factors will be limited to 20% (their Fig. 1, blue bar).

References

ABS (2013) *2011 Census Mesh Blocks*. Internet site http://www.abs.gov.au/ausstats/abs@.nsf/Latestproducts/1386.0MainFeatures3602013?opendocument&tabname=Summary&prodno=1386.0&issue=2013&num=&view, Canberra, Australia, Australian Bureau of Statistics.

Adams, A.S. and D.W. Keith (2013) Are global wind power resource estimates overstated? *Environmental Research Letters* 8, 015021.

AEMO (2010) *An introduction into Australia's National Electricity Market*. AEMO_0000-0262, Melbourne, Australia, Australian Energy Market Operator.

AEMO (2011) *Gas and electricity transmission comparative case study*. Chapter 8 National Transmission Network Development Plan, Australian Energy Market Operator.

AEMO (2012) *100 per cent renewables study - electricity transmission cost assumptions*. Internet site http://www.climatechange.gov.au/sites/climatechange/files/files/reducing-carbon/APPENDIX2-AEMO-transmission-cost-assumptions.pdf, Australian Energy Market Operator.

AEMO (2013) *100 per cent renewables study - modelling outcomes*. Internet site http://www.climatechange.gov.au/reducing-carbon/australian-energy-market-operator/100-cent-renewables-study-modelling-outcomes, Australian Energy Market Operator.

AEMO (2014a) *Aggregated Price and Demand Data - Historical*. Internet site http://www.aemo.com.au/Electricity/Data/Price-and-Demand/Aggregated-Price-and-Demand-Data-Files, Australian Energy Market Operator.

AEMO (2014b) *South Australian Electricity Market Economic Trends Report*. Australian Energy Market Operator Ltd.

AETA (2013) *Australian Energy Technology Assessment 2013 Model Update*. Internet site http://www.bree.gov.au/files/files//publications/aeta/AETA-Update-Dec-13.pdf, Canberra, Australia, Bureau of Resource and Energy Economics.

APVI (2014) *Solar Map: Mapping Australian Photovoltaic installations*. Internet site http://pv-map.apvi.org.au/historical - 4/-26.67/134.12, Australian PV Institute.

Bader, B.W. and T.G. Kolda (2007) Efficient MATLAB computations with sparse and factored tensors *SIAM Journal on Scientific Computing* 30, 205-231.

BREE (2013) *Australian energy statistics data*. Canberra.

Dobos, A.P. (2014) *PVWatts Version 5 Manual*. Technical Report NREL/TP-6A20-62641, Golden, USA, National Renewable Energy Laboratory.

EIA (2013) *Updated capital cost estimates for utility scale electricity generating plants*. Washington, DC, U.S. Energy Information Administration.

Elliott, D.L., C.G. Holladay, W.R. Barchet, H.P. Foote and W.F. Sandusky (1986) *Classes of wind power density at 10 m and 50 m*. Wind Energy Resource Atlas of the United States, Internet site http://rredc.nrel.gov/wind/pubs/atlas/tables/1-1T.html, Richland, USA, Pacific Northwest Laboratory.

Elliston, B., M. Diesendorf and I. MacGill (2012) Simulations of scenarios with 100% renewable electricity in the Australian National Electricity Market. *Energy Policy* 45, 606-613.

Elliston, B., I. MacGill and M. Diesendorf (2013) Least cost 100% renewable electricity scenarios in the Australian National Electricity Market. *Energy Policy* 59, 270-282.

EPA (2011) *Clean Energy Renewable Cost Data Base, 2008 – 2010*. Internet site http://www.epa.gov/cleanergy/documents/renewable_cost_datal.xls, Washington D.C., USA, Environmental Protection Authority.

Feldman, D., G. Barbose, R. Margolis, T. James, S. Weaver, N. Darghouth, R. Fu, C. Davidson, S. Booth and R. Wiser (2014) *Photovoltaic (PV) pricing trends: historical, recent and near-term projections*. National Renewable Energy Laboratory, Lawrence Berkeley National Laboratory.

Gary, J.A., K.H. Clifford, T.R. Mancini, G.J. Kolb, N.P. Siegel and B.D. Iverson (2010) *Development of a power tower technology roadmap for DOE*. Perpignan, France, SolarPaces.

Gilman, P. (2014) *SAM Photovoltaic Model (pvsamv1) Technical Reference*. Internet site https://sam.nrel.gov/sites/sam.nrel.gov/files/SAM%20DRAFT%20Photovoltaic%20Reference%20Manual%20May%2014%202014.pdf, Golden, USA, National Renewable Energy Laboratory.

Hinkley, J., B. Curtin, J. Hayward, A. Wonhas, R. Boyd, C. Grima, A. Tadros, R. Hall, K. Naicker and A. Mikhail (2011) *Concentrating solar power – drivers and opportunities for cost-competitive electricity*. Melbourne, Australia, CSIRO.

Holttinen, H. (2008) Estimating the impacts of wind power on power systems - summary of IEA Wind collaboration. *Environmental Research Letters* 3, 1-6.

Hoogwijk, M.M., B.J.M. De Vries and W.C. Turkenburg (2004) Assessment of the global and regional geographical, technical and economic potential of onshore wind energy. *Energy Economics* 26, 889-919.

Hoogwijk, M.M., D. Van Vuuren, B.J.M. De Vries and W.C. Turkenburg (2007) Exploring the impact on cost and electricity production of high penetration levels of intermittent electricity in OECD Europe and the USA, results for wind energy. *Energy* 32, 1381-1402.

Huang, J. (2014) Dynamic downscaling of Australian climate for solar energy resource assessment using CCAM. *AMOS National Conference 2014, 12-14 February 2014*. Hobart, Australia.

Huva, R., R. Dargaville and S. Caine (2012) Prototype large-scale renewable energy system optimisation for Victoria, Australia. *Energy* 41, 326-334.

IEA (2010) *Technology Road Map Concentrating Solar Power*. Internet site http://www.iea.org/publications/freepublications/publication/name,4010,en.html, Paris, France, International Energy Agency / OECD.

IRENA (2012a) *Renewable energy technologies: cost analysis series - hydropower*. International Renewable Energy Agency.

IRENA (2012b) *Renewable energy techologies: cost analysis series - concentrating solar power*. International Renewable Energy Agency.

IUCN (2014) *IUCN Protected Areas Categories System*. Internet site http://www.iucn.org/about/work/programmes/gpap_home/gpap_quality/gpap_pacategories/, Gland, Switzerland, IUCN.

IUCN and UNEP (2014) *World Database on Protected Areas*. Internet site http://www.protectedplanet.net/.

Jägemann, C., M. Fürsch, S. Hagspiel and S. Nagl (2012) *Decarbonizing Europe's power sector by 2050 - Analyzing the implications of alternative decarbonization pathways*. EWI Working Paper No 12/13, Köln, Germany, Energiewirtschaftliches Institut der Universität Köln.

Jorgenson, J., P. Denholm, M. Mehos and C. Turchi (2013) *Estimating the performance and economic value of multiple Concentrating Solar Power technologies in a production cost model*. Technical Report NREL/TP-6A20-58645, Golden, USA, National Renewable Energy Laboratory.

Kasten, F. and A.T. Young (1989) Revised optical air mass tables and approximation formula. *Applied Optics* 28, 4735–4738.

Lenzen, M., S. Jütte, B. McBain, T. Trainer, O. Rey-Lescure and J.R. Huang (2015) A new approach to optimal generator location for low-carbon power supply. to be submitted.

Lopez, A., B. Roberts, D. Heimiller, N. Blair and G. Porro (2012) *U.S. Renewable Energy Technical Potentials: A GIS-Based Analysis*. Technical Report NREL/TP-6A20-51946, Golden, USA, National Renewable Energy Laboratory.

Lovegrove, K., M. Watt, R. Passey, G. Pollock, J. Wyder and J. Dowse (2012) *Realising the Potential for Concentrating Solar Power in Australia*. Canberra, Australia, Australian Solar Institute.

Mason, I., S. Page and A. Williamson (2010) A 100% renewable electricity generation system for New Zealand utilising hydro, wind, geothermal and biomass resources. *Energy Policy* 38, 3973-3984.

McGregor, J.L. (2005) *C-cam: Geometric aspects and dynamical formulation*. Technical Paper 70, Canberra, Australia, CSIRO Marine and Atmospheric Research.

McGregor, J.L. and M.R. Dix (2008) An updated description of the conformal-cubic atmospheric model. In: K. Hamilton and W. Ohfuchi (eds.) *High-Resolution Simulation of the Atmosphere and Ocean*, Springer, 51-76.

Meibom, P., C. Weber, R. Barth and H. Brand (2007) Operational costs induced by fluctuating wind power production in Germany and Scandinavia. In: L. Sønderberg Petersen and H. Larsen (eds.) *Energy Solutions for Sustainable Development*. Roskilde, Denmark, Risø National Laboratory, 196-205.

Meinel, A.B. and M.P. Meinel (1976) *Applied Solar Energy*. Boston, USA, Addison Wesley Publishing Co.

Miller, L.M., N.A. Brunsell, D.B. Mechem, F. Gans, A.J. Monaghan, R. Vautard, D.W. Keith and A. Kleidon (2015) Two methods for estimating limits to large-scale wind power generation. *Proceedings of the National Academy of Sciences of the United States of America* 112, 11169-11174.

Miskelly, P. (2012) Wind farms in Australia - recent lessons. *Energy & Environment* 23, 1233-1260.

NREL (2010) *Job and Economic Development Impact (JEDI) model - default data*.

Orr, K. and N. Skeers (2014) *National Power Stations Database*. http://dx.doi.org/10.4225/25/544EE47D2C1DE, Canberra, Australia, Geoscience Australia.

PowerWater (2014) *Northern Territory Electricity Network*. Internet site https://http://www.powerwater.com.au/community_and_education/student_resources/maps/electricity_map, Darwin, Australia, Power and Water Corporation.

RAE (2014) *Wind turbine power calculations*. Internet site http://www.raeng.org.uk/publications/other/23-wind-turbine, London, UK, Royal Academy of Engineering.

Reda, I. and A. Andreas (2003) *Solar position algorithm for solar radiation application*. Technical report NREL/TP-560-34302, Golden, USA, National Renewable Energy Laboratory.

Resch, G., A. Held, T. Faber, C. Panzer, F. Toro and R. Haas (2008) Potentials and prospects for renewable energies at global scale. *Energy Policy* 36, 4048-4056.

Romero, R., A. Monticelli, A. Garcia and S. Haffner (2002) Test systems and mathematical models for transmission network expanion planning. *IEE Proceedings on Generation, Transmission and Distribution* 149, 27-36.

Short, W., P. Sullivan, T. Mai, M. Mowers, C. Uriarte, N. Blair, D. Heimiller and A. Martinez (2011) *Regional Energy Deployment System (ReEDS)*. Technical Report NREL/TP-6A20-46534, Golden, USA, National Renewable Energy Laboratory.

Tidball, R., J. Bluestein, N. Rodriguez and S. Knoke (2010) *Cost and performance assumptions for modeling electricity generation technologies*. Technical Report NREL/SR-6A20-48595, Golden, USA, National Renewable Energy Laboratory.

Turchi, C. (2010) *Parabolic trough reference plant for cost modeling with the Solar Advisor Model (SAM)*. Golden, USA, National Renewable Energy Laboratory.

Voorspools, K.R. and W.D. D'haeseleer (2006) An analytical formula for the capacity credit of wind power. *Renewable Energy* 31, 45-54.

WALIA (2010) *Western Australia energy resources and infrastructure*. Internet site https://http://www.finance.wa.gov.au/cms/uploadedFiles/Public_Utilities_Office/Energy_in_WA/OOE_Map_2010_A4_2.pdf, Perth, Australia, Western Australia Land Information Authority.

WMO (2003) *Manual on the Global Observing System - Volume I - Global Aspects*. Annex V to the WMO Technical Regulations WMO-No. 544, Geneva, Switzerland, World Meteorological Organization.